Behavioral/Cognitive

Proprioceptive and Visual Feedback Responses in Macaques Exploit Goal Redundancy

Kevin P. Cross,[1,2] Hui Guang,[2] and Stephen H. Scott[2,3,4]

[1]University of North Carolina Neuroscience Center, University of North Carolina School of Medicine, Chapel Hill, North Carolina 27599, [2]Centre for Neuroscience Studies, [3]Departments of Biomedical and Molecular Sciences, and [4]Medicine, Queen's University, Kingston, ON K7L 3N6, Canada

A common problem in motor control concerns how to generate patterns of muscle activity when there are redundant solutions to attain a behavioral goal. Optimal feedback control is a theory that has guided many behavioral studies exploring how the motor system incorporates task redundancy. This theory predicts that kinematic errors that deviate the limb should not be corrected if one can still attain the behavioral goal. Studies in humans demonstrate that the motor system can flexibly integrate visual and proprioceptive feedback of the limb with goal redundancy within 90 ms and 70 ms, respectively. Here, we show monkeys (*Macaca mulatta*) demonstrate similar abilities to exploit goal redundancy. We trained four male monkeys to reach for a goal that was either a narrow square or a wide, spatially redundant rectangle. Monkeys exhibited greater trial-by-trial variability when reaching to the wide goal consistent with exploiting goal redundancy. On random trials we jumped the visual feedback of the hand and found monkeys corrected for the jump when reaching to the narrow goal and largely ignored the jump when reaching for the wide goal. In a separate set of experiments, we applied mechanical loads to the arm of the monkey and found similar corrective responses based on goal shape. Muscle activity reflecting these different corrective responses were detected for the visual and mechanical perturbations starting at ~90 and ~70 ms, respectively. Thus, rapid motor responses in macaques can exploit goal redundancy similar to humans, creating a paradigm to study the neural basis of goal-directed motor action and motor redundancy.

Key words: **macaque; OFC; proprioception; redundancy; vision**

Significance Statement

Moving in the world requires selecting from an infinite set of possible motor commands. Theories predict that motor commands are selected that exploit redundancies. Corrective responses in humans to either visual or proprioceptive disturbances of the limb can rapidly exploit redundant trajectories to a goal in <100 ms after a disturbance. However, uncovering the neural correlates generating these rapid motor corrections has been hampered by the absence of an animal model. We developed a behavioral paradigm in monkeys that incorporates redundancy in the form of the shape of the goal. Critically, monkeys exhibit corrective responses and timings similar to humans performing the same task. Our paradigm provides a model for investigating the neural correlates of sophisticated rapid motor corrections.

Introduction

A common problem in motor control concerns how to select muscle commands when there are many different ways to attain a behavioral goal (Bernstein, 1967; Flash and Hogan, 1985; Sporns and Edelman, 1993; Scholz and Schöner, 1999; Scholz et al., 2000; Latash, 2012). For example, successfully reaching for an object can involve many different trajectories of the limb to the goal and, thus, many different patterns of muscle activity. Optimal feedback control (OFC) provides a framework for how to select motor commands among a family of redundant solutions (Todorov and Jordan, 2002; Scott, 2004). OFC selects motor commands to optimize a cost function that balances successfully completing the behavioral goal with the cost of movement (e.g., energy, noise). Importantly, these controllers abide by

Received July 7, 2022; revised Dec. 7, 2022; accepted Dec. 10, 2022.

Author contributions: K.P.C. and S.H.S. designed research; K.P.C. and H.G. performed research; K.P.C. and S.H.S. contributed unpublished reagents/analytic tools; K.P.C. analyzed data; and K.P.C. and S.H.S. wrote the paper.

This work was supported by Canadian Institutes of Health Research Grant PJT-159559 to S.H.S. K.P.C. was supported by an Ontario Graduate Scholarship, and S.H.S. was supported by a GlaxoSmithKline–Canadian Institutes of Health Research Chair in Neurosciences. We thank Kim Moore, Simone Appaqaq, Catherine Crandell, Jordan Miller, Ethan Heming, and Helen Bretzke for laboratory and technical assistance.

S.H.S. is cofounder and Chief Scientific Officer (CSO) of Kinarm, which commercializes the robotic technology used in the present study. The other authors declare no competing financial interests.

Correspondence should be addressed to Kevin P. Cross at 13kc18@queensu.ca.

https://doi.org/10.1523/JNEUROSCI.1332-22.2022

the minimum intervention principle where kinematic errors that arise during movement are only corrected if they interfere with the behavioral goal. Or alternatively stated, errors that deviate the plant along redundant trajectories should not be corrected. As a result, variability accumulates along redundant task dimensions.

Several studies demonstrate that the motor system exploits task redundancies similar to OFC controllers (Diedrichsen, 2007; Dimitriou et al., 2012; Cluff and Scott, 2015; Weiler et al., 2015, 2016). A common approach is to have participants reach to a spatially redundant goal such as a wide rectangular bar (Knill et al., 2011; Nashed et al., 2012; de Brouwer et al., 2017; Keyser et al., 2017, 2019; De Comite et al., 2021). Participants exhibit greater trial-to-trial variability in their reach endpoints when reaching for a wide goal as compared with a narrow goal. The increased variability exhibits structure as variability primarily accumulates along the wide (redundant) axis of the goal. Furthermore, displacements to the visual feedback of the hand (cursor jump) are fully corrected by participants when reaching for a narrow goal and are corrected less when reaching for the wide goal if the displacement is along the redundant axis (Knill et al., 2011; de Brouwer et al., 2017; Cross et al., 2019). Differences in these corrective responses arise in muscle activity ~90 ms after the jump (Franklin and Wolpert, 2008; Cross et al., 2019). Similar corrective responses occur when mechanical loads are applied to the limb with differences between corrective responses starting ~70 ms after the load (Nashed et al., 2012; Lowrey et al., 2017; Keyser et al., 2019). However, despite the prevalence of OFC as a theory of motor control, we know little about the neural circuits used to generate OFC-like behaviors.

One challenge with investigating neural circuits underlying rapid motor responses is that behavioral tasks must be translated into animal models that allow for invasive neural recordings such as rhesus monkeys or rodents. To perform most behavioral tasks the behavior of the animal must be shaped using reward over the course of tens of thousands of trials. This excessive training along with behavioral shaping results in behavior that is highly reproducible on a trial-by-trial basis, which provides advantages when analyzing noisy neural activity. However, it is unclear if this highly reproducible behavior comes at the cost of behavioral flexibility. For example, Bizzi et al. (1982, 1984) trained monkeys to reach to a goal and applied an assistive mechanical load that pushed the limb of the monkey toward the goal. Monkeys corrected by actively resisting the load in what appeared to be an attempt to return the limb to the original trajectory to the goal. In contrast, OFC models and humans performing a similar task do not return to the original trajectory and instead allow the load to push the hand toward the goal, thereby exploiting the fact that there are redundant trajectories (Cluff and Scott, 2015). Thus, humans can exploit task redundancies; however, it is unclear whether monkeys are capable of exploiting redundancies in an experimental setting because of overtraining and behavioral shaping.

Here, we investigated whether monkeys could learn to exploit the spatial redundancy of a goal during reaching. We found monkeys exhibited greater variability in their reach endpoints on unperturbed trials. Further, monkeys corrected less for visual and mechanical perturbations of the limb when reaching for the spatially redundant target, consistent with exploiting goal redundancy. Muscle recordings indicated that feedback responses to visual and mechanical perturbations reflected goal redundancy within <100 ms.

Materials and Methods

Four male monkeys (*Macaca mulatta*, 10–20 kg) were trained to sit in a primate chair and place their upper arm into a robotic exoskeleton (Kinarm; Scott, 1999). The robot constrained the arm of the monkey to move in a two-dimensional plane and included a virtual reality system that could display virtual targets and visual feedback of the limb. Experiments were approved by the Queen University Research Ethics Board and Animal Care Committee.

Behavioral task for visual perturbations

Monkeys were trained to make goal-directed reaches to targets in the virtual environment. Visual feedback of the hand was provided by a white cursor (radius, 0.8 cm) aligned with the index fingertip of the monkey. At the start of each trial, a start target (square, side length, 1.2 cm) appeared and the monkey was required to reach and hold its hand at the target for 750–1500 ms. Next, a goal target appeared that was located 8 cm lateral and 4.4 cm in front of the start goal (total reach distance, 9.2 cm; Fig. 1*A*). To reach the goal from the starting position, monkeys had to primarily extend their elbow. When the hand of the monkey left the start target, they had 900 ms to reach and stabilize their hand within the goal for 500 ms. The goal could either be a narrow rectangle (length, 2 cm; width, 2.2 cm) or a wide rectangle with its long axis oriented perpendicular to the reach axis (length, 12 cm; width, 2.2 cm). On random trials, the cursor jumped orthogonal to the reach axis (orthogonal reach axis) once the hand was 2 cm from the start target, and on these trials monkeys were given an additional 500 ms to reach the goal. For monkeys M and A, the cursor jumped ±4 cm, and for monkeys T and C the cursor jumped ±3.5 cm. Within a block of trials there were six no-jump reaches (three for both goal shapes), and four cursor-jump trials (2 directions × 2 goal shapes). Monkeys completed 10–25 blocks in a recording session resulting in ~60–150 unperturbed trials and 40–100 perturbed trials.

Behavioral task for mechanical perturbations

The task was similar to the cursor perturbation task, but there were several changes to the shape and size of the goal targets. First, the size of the redundant axis of the wide goal was 28 cm long (Fig. 1*B*), and it was shaped like an arrowhead composed of two rectangles overlapping at the edges and at an angle of 110° with respect to each other. We chose this configuration as it brought the edges of the goal closer in proximity to the arm of the monkey, thus making it easier to reach on perturbation trials. On random trials mechanical loads were applied to the joints to displace the limb approximately orthogonal to the reach axis (monkeys M, A, T, C pushes limb away from body, shoulder 0.5, 0.45, 0.4, 0.3 Newton meters (Nm); elbow 0, 0, 0, 0 Nm; pushes limb toward the body, shoulder −0.5, −0.45, −0.4, −0.3 Nm; elbow 0.15, 0.1, 0.07, 0.14 Nm; plus flexion loads, minus extension loads). Because of the influence of limb mechanics (i.e., limb inertia, limb geometry), loads were adjusted for each monkey to generate roughly similar hand deviations. Cursor feedback was temporarily removed for 200 ms when a load was triggered on perturbation trials and on unperturbed trials at the equivalent time point for when a load would have been applied. The temporary removal of visual feedback ensured evoked muscle activity was the result of proprioceptive feedback while still allowing the animal terminal visual feedback of their hand to reach the goal. We also increased the number of unperturbed trials to reduce anticipatory corrections to the mechanical loads. Within a block of trials there were eight no-load reaches (four for both goal shapes), and four load trials (2 directions × 2 goal shapes). Monkeys completed 10–15 blocks in a given recording session resulting in ~80–120 unperturbed trials and 40–60 perturbed trials.

Note that before learning either variant of the task, monkeys had varying degrees of experience (2–3 months up to 8+ years) with tasks involving reaching to small targets in the virtual environment and countering loads applied to their limb. When they were first trained on the present tasks, they were presented the two goal shapes to reach toward without any perturbations. This initial familiarization lasted for a few days on which perturbations were introduced. Importantly, during training we administered water reward if the animal was successful regardless

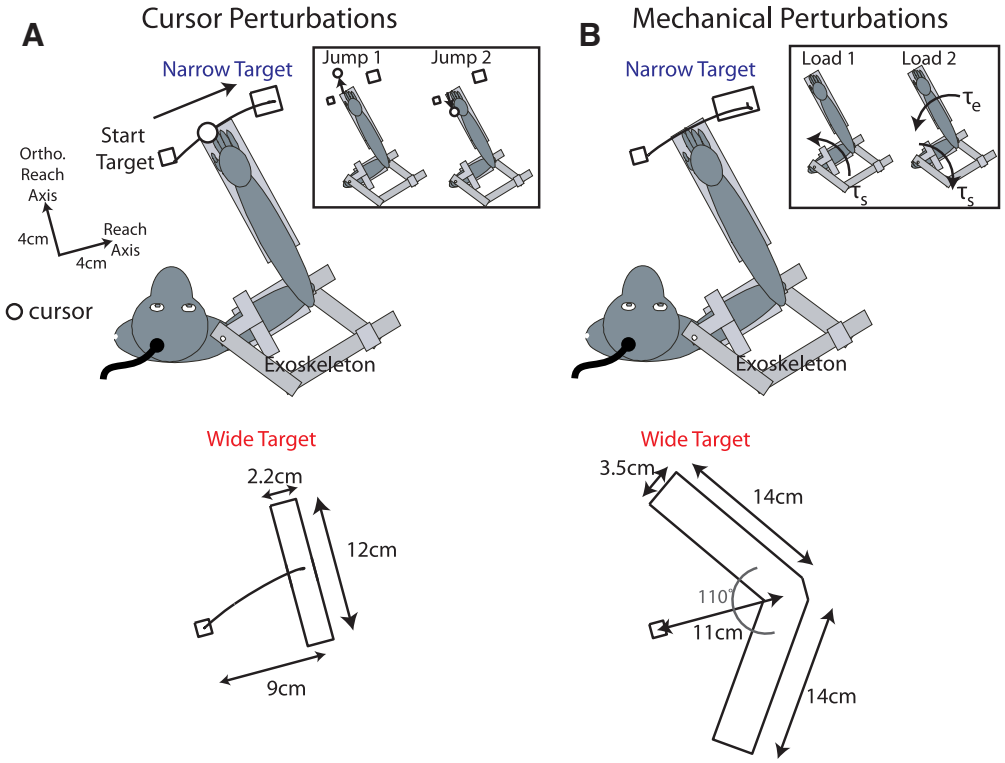

Figure 1. Experimental setup. ***A***, Monkeys placed their arm inside a robotic exoskeleton and were trained to reach from a starting position (Start Target) to either a narrow target (top) or wide target (bottom). Inset, on random trials, the visual feedback of the hand (cursor) jumped orthogonally by 3–4 cm (see above, Materials and Methods, Behavioral task for visual perturbations). ***B***, Same as ***A*** showing the configuration of the targets during the mechanical perturbation experiment. Inset, on random trials, mechanical loads were applied to the limb that displaced the limb orthogonally.

of the location on the goal it reached for to minimize any biases we had on the behavior of the animal.

Estimating visual onsets

On cursor-jump trials, there is an ~20–49 ms delay between when the command was sent to jump the cursor and when it actually updated the screen. We estimated this delay on a trial-by-trial basis by using photodiodes placed at the side of the screen and flashing white squares coincident to the photodiode locations when the cursor jumped.

Muscle recordings

We implanted monkey M with a 32-channel chronic EMG system (Link-32, Ripple Neuro). The system had eight leads that were inserted into the muscle belly and were attached to a processor. Each lead had four separate contacts for recording intramuscular activity (impedance 20 kOhm). The processor was implanted under the skin and located near the midline of the back at the midthoracic level. Muscles implanted were brachioradialis (Brd), brachialis (Br), the lateral(TLat) and long heads of the triceps (TLong), biceps (long head, Bi), pectoralis major (PM), and anterior and posterior deltoids. An external receiver was secured to the skin over the processor using magnets in the receiver and processor. The external receiver was capable of powering the internal processor, and EMG signals were transmitted through the skin from the processor to the receiver by photodiodes. The signals were then relayed to the Grapevine Neural Interface Processor (Ripple Neuro), bandpass filtered (15–375 Hz) and recorded at 2 kHz.

In monkey C we recorded muscle activity using surface EMG electrodes (Delsys). We recorded activity from brachialis, biceps, and the lateral and long head of the triceps. Activity was sampled at 1 kHz.

Kinematic recordings

The shoulder and elbow angles, angular velocities, and angular accelerations were recorded by either a 128 Channel Neural Signal Processor (Blackrock Microsystems) at 1 kHz or by the Grapevine Neural Interface Processor at 30 kHz.

Data and statistical analyses

Kinematic analysis

The endpoint position of the reach was calculated by finding the hand position at the end of the trial (time point after 500 ms hold period). This hand position was then projected onto the redundant axis of the wide goal by finding the location on the redundant axis that had the shortest distance to the hand position.

We estimated the timing of the kinematic corrections using the hand velocity along the orthogonal reach axis, which was defined as the velocity component perpendicular to the straight path connecting the start and middle of the goal (Fig. 1, reach axis). The hand velocity was aligned to the onset of the perturbation (cursor jump or mechanical load) or the equivalent time point on no-perturbation trials (faux jump or faux load). The average velocity for no-perturbation trials was subtracted from the velocity for perturbation trials resulting in the change (Δ) in hand velocity. Timing of when the hand velocity differentiated based on goal shape was determined using receiver operating characteristics (ROCs; Corneil et al., 2004; Gu et al., 2016; Pruszynski et al., 2016; Cross et al., 2019). At each time point we generated an ROC curve between the hand velocities for the narrow and wide goals. The area under the ROC curve reflects how discriminable the trials for the narrow and wide goals are and can range from 0.5, indicating chance discrimination, to 0 and 1 indicating perfect discrimination. We found the first time point that had an area $>0.8/<0.2$ and that was maintained above this threshold for 10 consecutive time points (10 ms). We then traced backward in time to the first time point that fell below/above 0.6/0.4 (knee). Note, our ROC analysis assumes the data are normally distributed, which is a common assumption for kinematic data (Corneil et al., 2004; Gu et al., 2016; Pruszynski et al., 2016).

EMG analysis

For indwelling muscle activity recorded from monkey M we down sampled activity to 1 kHz. For each lead containing four electrodes, we

computed differential signals from the two most proximal contacts and two most distal contacts relative to the processor. This resulted in two samples recorded from each muscle resulting in a total of 16 total samples (2 × 8 muscles recorded = 16 total samples). Trials recorded from across days were pooled.

For muscle activity recorded using surface electrodes from monkey C, we only included recordings from days where perturbation-related activity was detected (see below, Preferred direction and perturbation-sensitive criteria). This was necessary as the surface electrodes would frequently lose contact with the skin during the recording or would shift resulting in poor signal-to-noise ratio. For the visual perturbation experiment we included 4, 1, 3, and 3 recording sessions for the brachialis, biceps, triceps lateral head, and triceps long head, respectively. For the mechanical perturbations experiment, we included 4, 3, 6, and 6 recording sessions for the brachialis, biceps, triceps lateral head, and triceps long head, respectively. Within a recording session we also rejected trials if the perturbation-evoked activity was >3 SDs for a given day to remove trials where the electrode temporarily lost contact with the skin and only constituted 0–4% of trials. Trials recorded from across days were pooled. Note, the removal of these trials along with sessions with poor signal to noise did not substantially have an impact on the general activity profiles for each muscle but did have an impact on the ability of our statistical tests to determine significance (data not shown).

The differential signals were rectified and low-pass filtered with a sixth-order zero-phase lag Butterworth filter at 50 Hz. Note that this low-pass filtering step was necessary for determining the timing of the evoked responses and is similar to our previous approach (Lowrey et al., 2017; Cross et al., 2019; Kasuga et al., 2022). Muscle activities were aligned to the onset of the perturbation. Muscle activities were then trial averaged, and the activities on no-perturbation trials were subtracted from perturbation trials to yield the change in activity caused by the perturbation. Muscle activities were normalized by the mean perturbation-related activity from 0 to 300 ms after perturbation onset.

Analysis of no-perturbation trials

We compared magnitudes of muscle activity between reaches for the narrow and wide goals on no-perturbation trials. Activities were averaged in the epoch starting 200 ms before the faux-jump/faux-load onset until 200 ms after the onset (movement epoch). A two-sample t test identified muscles that were significantly different between the narrow and wide goals ($p < 0.01$). We also examined the temporal correlation of muscle activities between the narrow and wide goals during the movement epoch using Pearson's correlation coefficient. We compared the observed distribution across muscles with a shuffled distribution, where correlations were computed between randomly selected muscles.

Preferred direction and perturbation-sensitive criteria

The preferred perturbation direction of a muscle was calculated by averaging the perturbation-related activities over the first 300 ms after the perturbation onset for reaches to the narrow goal. The direction with the largest activity over this epoch was defined as the preferred direction. The same preferred direction was used for both the narrow and wide goals.

Perturbation-sensitive muscle samples were identified using a two-sample t test comparing the activity on unperturbed trials with activity on perturbation trials in the preferred direction of the muscle in the epoch of 0–300 ms after the perturbation onset. This was applied twice for each muscle, one test for each target shape. Muscles were classified as perturbation sensitive if $p < 0.05$ (Bonferroni correction factor 2).

Epoch analysis

We compared how perturbation-related activities differed between goal shapes over time. For the mechanical perturbations we divided the activity of each muscle into epochs of 20–50, 50–75, 75–100, and 120–180 ms based on previous work (Lee and Tatton, 1975; Crago et al., 1976; Bonnet, 1983; Omrani et al., 2014; Pruszynski et al., 2014). For the cursor perturbations we considered the same epochs but shifted 50 ms forward in time (70–100, 100–125, 125–150, and 170–230 ms) to account for the fact that corrective muscle activity to visual feedback starts ~50 ms slower than for proprioceptive feedback (Franklin and Wolpert, 2008; Pruszynski et al., 2010, 2016; Dimitriou et al., 2013; Cross et al., 2019).

Population signal

We calculated the population signal by averaging the activities for all perturbation-sensitive muscle samples in their preferred directions. A difference signal was calculated by subtracting the activities for the wide goal from the narrow goal for all perturbation-sensitive muscle samples followed by averaging across samples. The onset for the population signals were estimated by calculating the mean and SD of the baseline activity (300 ms before perturbation onset) and finding the first time point that exceeded the mean by 3 SDs for 20 consecutive time points (Omrani et al., 2016).

Statistics

Statistical comparisons of the reach endpoint positions between the narrow and wide goals were assessed using paired t tests. A Bonferroni correction factor of 2 was applied when comparing perturbation trials to account for the two perturbation directions. A one-way ANOVA was applied for comparing timing onsets (three levels, earliest onset for narrow goal, earliest onset for wide goal, task onset), and *post hoc* two-sample t tests were used to compare between levels with a Bonferroni correction factor of 3.

Statistical comparisons of muscle activity across epochs were assessed using a two-way repeated-measures ANOVA with epoch (four levels; see above, Epoch analysis) and goal shape (2 levels, narrow and wide) as factors. The ANOVA was significant if there was a main effect of goal shape, or the interaction effect was significant (Bonferroni correction factor of 2). *Post hoc* paired t tests were used to compare goal shape in each epoch (Bonferroni correction factor of 4). Muscle activity on unperturbed trials was assessed using paired t tests.

In line with previous studies (Nashed et al., 2012, 2014; Cluff and Scott, 2015; Cross et al., 2019), we assessed statistical significance using parametric statistics, and the threshold for significance was set as $p < 0.05$. However, we also assessed significance using appropriate nonparametric statistics and found nearly the same results, indicating our findings are robust to statistical methods (data not shown).

Results

Our goal was to develop a reaching task to examine whether monkeys could exploit the spatial redundancy of a goal. The original tasks performed by humans involved a multijoint reach directly in front of the shoulder joint (Nashed et al., 2012; Cross et al., 2019). However, our initial attempt to translate this task into the monkey was not successful as the monkey exhibited substantial bias toward reaching one end of the bar (Note that humans can also show a similar bias, albeit smaller; Keyser et al., 2017). Instead, we focused on reaches that primarily required an elbow extension movement, which produced more consistent behavior (Fig. 1). Below, we first describe the experiments that involved cursor perturbations followed by the experiments that involved mechanical perturbations.

Experiment 1: goal redundancy and feedback responses to cursor jumps

We trained four monkeys to reach to a goal that could be either a narrow square (Fig. 1*A*, top) or a wide rectangle (Fig. 1*A*, bottom; trials interleaved). For monkeys M, A, T, and C, we recorded 6, 7, 14, and 12 behavioral sessions of the animals performing the task on separate days that were spread across 1–2 years for each monkey, and monkeys were able to perform the task with high efficiency (success rates across all trial types, monkeys M, A, T, C, narrow targets = 95, 98, 89, 97%; wide targets = 96, 100, 92, 98%).

Figure 2*A* shows the hand paths for monkey M to the narrow (left) and wide (right) goals from one recording session. There was greater trial-by-trial variability in the hand position during

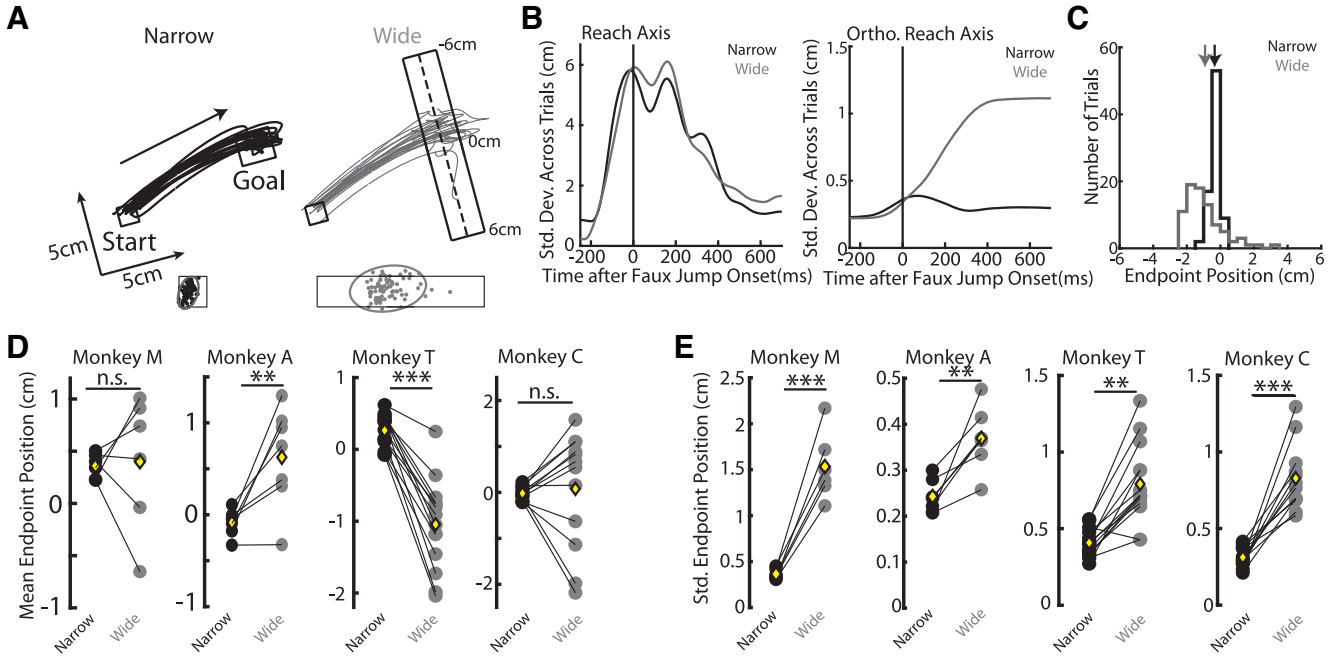

Figure 2. Example kinematics on unperturbed trials for the cursor-jump variant of task. ***A***, Top, Hand paths from one session for monkey M to the narrow (left) and wide (right) goals. Arrow denotes the direction of reach. Dashed line on the wide goal denotes the redundant axis. Bottom, Reach endpoints and the 95% confidence ellipse. ***B***, SDs of the hand position across trials for the narrow and wide goal reaches. ***C***, Reach endpoint histograms for reaches to the narrow and wide goals from the same session as ***A***. Zero denotes the middle of the redundant axis (***A***, middle of dashed line). Arrows denote the means of the distributions. ***D***, The mean endpoint position for the narrow and wide goals across all recording sessions. Yellow diamonds denote the means across sessions. Each session contained 30–75 reaches for each goal shape. ***E***, Same as ***D*** for SD of the endpoint positions. Hand paths on cursor-jump trials from the same session as ***A***. $^{**}p < 0.01$, $^{***}p < 0.001$. From the same recording session with 80 unperturbed trials each for the narrow and wide goals (***A–C***).

the reach to the wide goal, whereas variability was considerably smaller during reaches to the narrow goal. This resulted in the reach endpoints exhibiting greater dispersion along the redundant axis of the goal for reaches to the wide goal compared with reaches to the narrow goal (Fig. 2*A–C*). Across recording sessions, there was no significant difference in mean endpoint position for monkeys M and C, whereas there was a 0.7 cm and 1.3 cm difference between endpoint positions for the narrow and wide goals for monkeys A ($t_{(6)} = 3.8$, $p = 0.01$; Fig. 2*D*) and T ($t_{(13)} = 9.5$, $p < 0.001$), respectively. In contrast, the SD of the reach endpoints were 4.2, 1.5, 2.0, and 1.9 times greater for the wide goal than the narrow goal for monkeys M, A, T, and C, respectively (Fig. 2*E*; paired *t* test, monkeys M, A, T, C, $t_{(5)} = 8.3$, $t_{(6)} = 4.6$, $t_{(13)} = 6.8$, $t_{(11)} = 10.9$; $p < 0.001$, $p = 0.004$, $p < 0.001$, $p < 0.001$).

Next, we examined the unperturbed hand velocities for reaches to the narrow and wide goals. Figure 3, *A* and *B* (insets), show the unperturbed hand velocities during the same recording session along the reach and the orthogonal reach (Ortho. Reach) axes, respectively. There was a small increase in the peak hand velocity for reaches to the wide goal compared with reaches to the narrow goal. Across recording sessions, we found a small increase in hand speed for the wide goal for monkey M (narrow = 0.48 m/s, wide = 0.51 m/s; paired *t* test, $t_{(5)} = 3.6$, $p = 0.02$), a small decrease for the wide goal for monkey T (narrow = 0.35 m/s, wide = 0.32 m/s; $t_{(13)} = 2.5$, $p = 0.02$), and no effect of goal shape on hand speed for monkeys A and C (narrow = 0.52, 0.49 m/s, wide = 0.52, 0.5 m/s, $t_{(6)} = 2.0$, $t_{(11)} = 0.2$, $p = 0.1$, $p = 0.8$).

Next, we examined how goal redundancy affected corrective responses for unexpected cursor jumps. Figure 4*A* shows hand paths of monkey M on cursor-jump trials for the narrow and wide goals. There is a clear correction for the cursor jump when reaching for the narrow goal without substantial overshooting of the goal likely because of the extensive training the animals had in the task. In contrast, there was little if any correction when reaching for the wide goal. There was also greater trial-by-trial variability in the hand position during the reach to the wide goal (Fig. 4*B*), indicating that the monkey did not simply learn to reach for a particular location on the goal during cursor-jump trials. We calculated the differences between reach endpoints on cursor-jump trials and the mean of the unperturbed reach endpoint (change in reach endpoint; Fig. 4*C*). For the narrow goal, the change in reach endpoints for either cursor jump direction (Fig. 4*C*, blue solid line, jumps away from body; blue dashed line, jumps toward body) were narrow distributions centered near zero (mean, solid 0.26 cm; dashed −0.55 cm) indicating that monkeys ended their reach at almost the same location as on unperturbed trials. In contrast, for the wide goal, the change in reach endpoints generated wide distributions that were centered ~3 cm from the zero mark (Fig. 4*C*, red solid 2.9 cm, red dashed −3.6 cm) indicating that the monkey largely ignored the cursor jump. Across sessions and in both jump directions, there was a greater change in endpoint position for the wide goal than the narrow goal (Fig. 4*D*,*F*; paired *t* tests, jumps away from body, toward body, monkey M, $t_{(5)} = 7.6$, $t_{(5)} = 11$, $p = 0.00$, $p < 0.001$; monkey A, $t_{(6)} = 49$, $t_{(6)} = 48.9$, $p < 0.001$, $p < 0.001$; monkey T, $t_{(13)} = 33$, $t_{(13)} = 19$, $p < 0.001$, $p < 0.001$; monkey C, $t_{(11)} = 24$, $t_{(11)} = 23.8$, $p < 0.001$, $p < 0.001$, Bonferroni correction factor of 2). Furthermore, the SD in reach endpoints was also significantly greater for reaches to the wide goal for monkey M (Fig. 4*E*,*G*; jumps away from body, toward body, paired *t* test, $t_{(5)} = 7.9$, $t_{(5)} = 8.4$, $p = 0.001$, $p < 0.001$, Bonferroni correction factor 2), monkey T ($t_{(13)} = 6.4$, $t_{(13)} = 5.6$, $p < 0.001$, $p < 0.001$), and monkey C ($t_{(11)} = 8.4$, $t_{(11)} = 7.1$, $p < 0.001$, $p < 0.001$). For monkey A, a significant increase in the SD in reach endpoints was found for jumps toward the body ($t_{(6)} = 8.6$, $p < 0.001$) but not for jumps

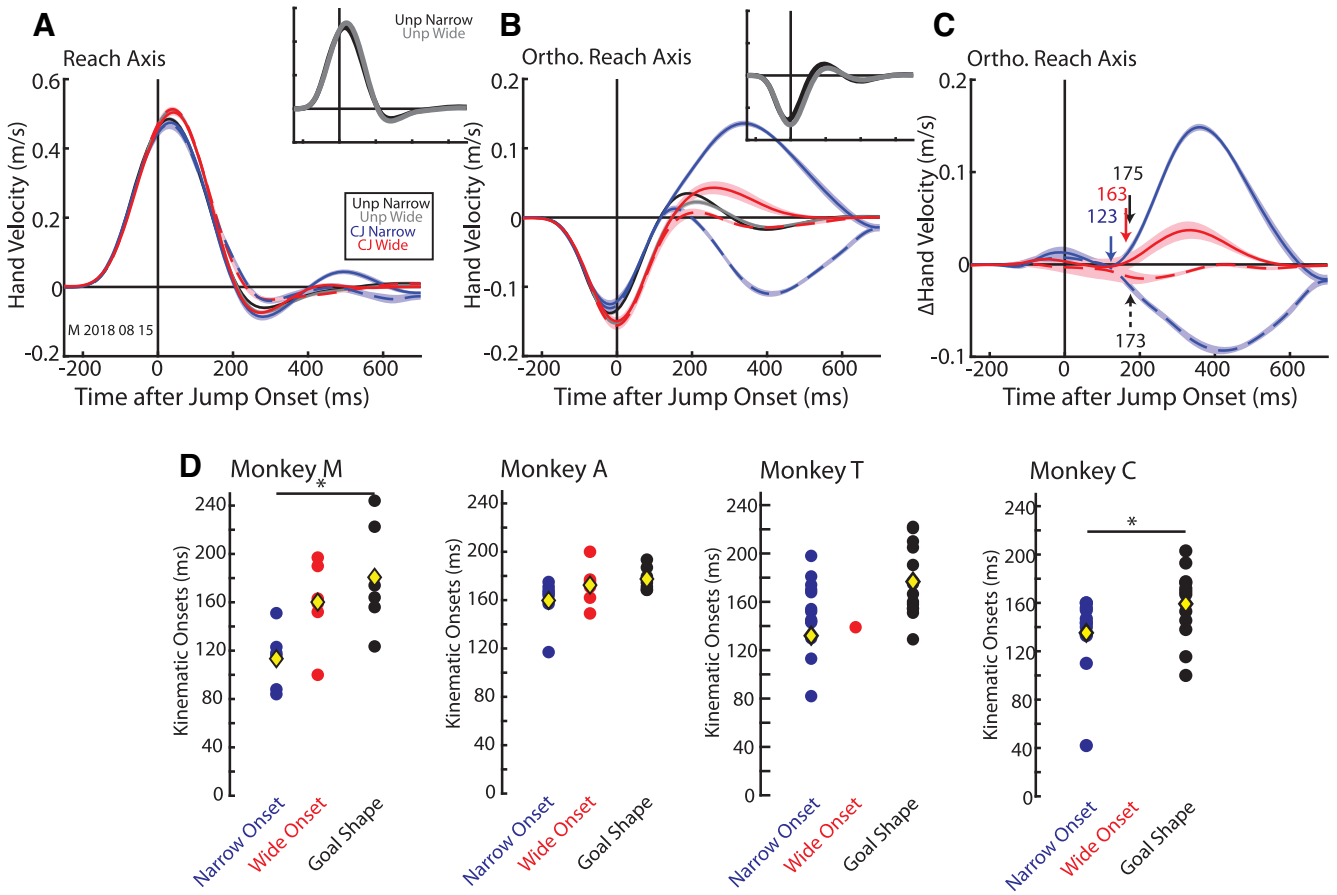

Figure 3. Example hand velocity profiles for the cursor-jump variant of task. ***A***, The hand velocity along the reach axis (Fig. 1) for the narrow and wide goals. Velocity was aligned to the jump onset. Inset, The unperturbed reaches to the narrow and wide goals. Unp Narrow and Unp Wide, unperturbed reaches to the narrow and wide goals, respectively. CJ Narrow and CJ Wide, cursor jump trials for reaches to the narrow and wide goals, respectively. Solid and dashed lines denote cursor jumps away from the body and toward the body, respectively. ***B***, Same as ***A*** for the hand velocity along the orthogonal reach axis. ***C***, The change in the hand velocity on cursor-jump trials for the narrow and wide goals. Blue and red arrows denote the earliest corrective onset for the narrow and wide goals, respectively. Black arrows denote when corrective movements differentiate based on goal shape. ***D***, The earliest corrective onsets for the narrow (blue) and wide goals (red) along with the onsets for when corrections differentiated based on goal shape (black) across sessions. Yellow diamonds are the means across sessions. Each session contained 10–25 perturbed trials for each perturbation direction and goal shape and 30–75 unperturbed trials for each goal shape. $*p < 0.05$. From the same recording session as Figure 2, *A* and *C*, with 20 perturbed trials for each perturbation direction and goal shape and 80 unperturbed trials for each goal shape (***A–C***).

away from the body ($t_{(6)} = 1.6$, $p = 0.4$). Thus, reach endpoints on cursor-jump trials were more variable and biased toward the edges of the goal during wide goal reaches as compared with narrow goal reaches.

For cursor-jump trials, kinematic changes were primarily restricted to the orthogonal reach axis, which coincided with the direction in which the cursor jumped (Fig. 3*A*,*B*). Figure 3*C* shows the hand velocity after subtracting the unperturbed hand velocity (Δortho reach velocity). For the narrow and wide goals, the monkey initiated a correction for the cursor jump within 123 ms (blue arrow, narrow onset; identified using ROC analysis, see above, Materials and Methods) and 163 ms (red arrow, wide onset) of the jump onset, respectively. Differences between corrective responses for the narrow and wide goals began to differentiate ~174 ms after the jump (solid and dashed black arrows; goal shape onset). Across recording sessions, monkeys M and A initiated a correction within 113 and 160 ms and 160 and 173 ms of the cursor jumps to the narrow and wide goals, respectively. Monkeys C and T initiated a correction for the narrow goal 132 and 135 ms after jump onset but did not reliably detect a correction for the wide goal. Hand velocity differentiated based on goal shape starting at 181, 178, 176 and 159 ms (average across both directions; Fig. 3*D*) for monkeys M, A, T, and C. A one-way repeated-measures ANOVA with onset type as a factor (three levels, narrow and wide goals, and goal shape) was significant for monkey M ($F_{(2,10)} = 5.0$, $p = 0.03$). *Post hoc* paired *t* tests revealed a significant difference between the narrow onset and the goal-shape onset ($t_{(5)} = 4.1$, $p = 0.02$, Bonferroni correction factor of 3). The ANOVA was not significant for monkey A ($F_{(2,12)} = 2.3$, $p = 0.14$). Because the wide goal onsets were largely absent for monkeys T and C, we instead used paired *t* tests between the narrow and goal shape onsets and found onsets were not significant (monkeys T and C, $t_{(13)} = 2.0$, $t_{(11)} = 2.0$, $p = 0.06$, $p = 0.07$).

From monkey M, we implanted an indwelling chronic EMG system that recorded the activities of eight muscles that spanned the shoulder and elbow joints. The system allowed us to sample activity from each muscle twice (2 samples × 8 muscles = 16 total samples) and allowed us to record the same muscle across multiple recording sessions (see above, Materials and Methods). We recorded muscle activities across two sessions and pooled trials. As we were largely interested in perturbation-related activity, we restricted our analysis to 14 of 16 samples that responded to the cursor jump (see above, Materials and Methods, Preferred

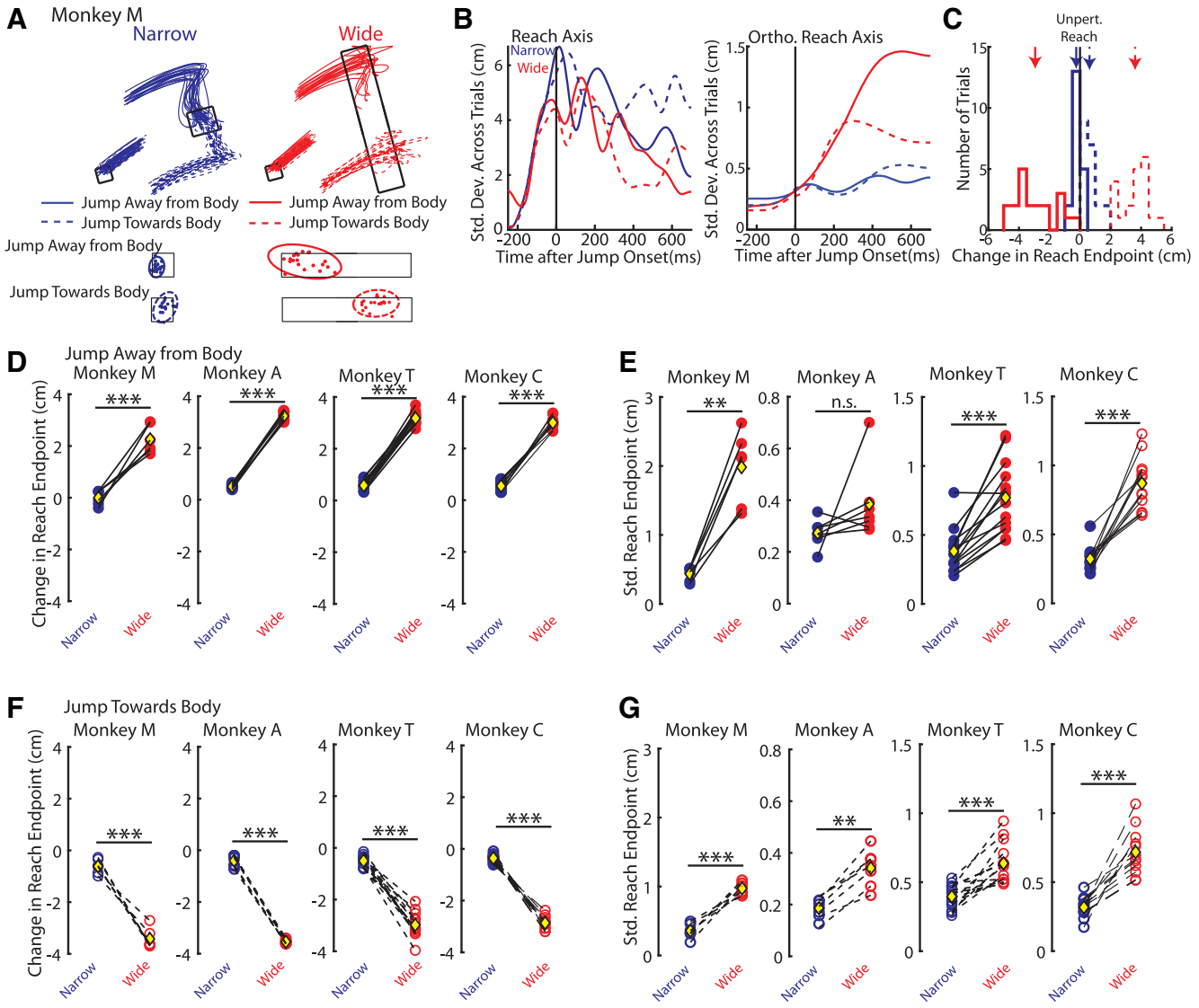

Figure 4. Example kinematics on cursor-jump trials. ***A***, Top, Hand paths from monkey M for cursor-jump trials. Bottom, Reach endpoints and the 95% confidence ellipse. Solid and dashed lines denote cursor jumps away from the body and toward the body, respectively. ***B***, SD of the hand position across trials for the narrow and wide goal reaches. ***C***, The change in reach endpoint histograms (change relative to unperturbed reach trials). Zero denotes the mean of the reach endpoints on unperturbed trials (Fig. 2*C*, arrows). Arrows denote the means of the distributions. ***D***, The mean change in reach endpoint for jumps away from the body across all recording sessions. Each session contained 10–25 perturbed trials for each perturbation direction and goal shape. ***E***, Same as ***D*** for the SD in reach endpoints. ***F***, ***G***, Same as ***D***, ***E*** for jumps toward the body. $^{**}p < 0.01$, $^{***}p < 0.001$. From same recording session as Figure 2, *A–C*, with 20 perturbed trials for each perturbation direction and goal shape (***A–C***).

direction and perturbation-sensitive criteria). For monkey C, we recorded muscle activity using surface electrodes over the course of four sessions. We only analyzed recording days where perturbation-related activity was detected in a given muscle (number of good sessions, TLat, 3; Br, 4; Bi, 1; TLong, 3) as the surface electrodes had a tendency to lose contact during a recording as well as the variability inherent in day-to-day electrode placements.

Figure 5*A* shows the average activity on unperturbed trials for the pectoralis major (PM; shoulder flexor) muscle aligned to the faux-jump onset from monkey M. The temporal structure of the muscle activity was comparable between goal shapes; however, starting around the time of the faux-jump onset there was a greater increase in activity for the narrow goal than the wide goal. In contrast, the long head of the triceps (shoulder and elbow extensor) exhibited similar temporal structure and activity magnitudes for the narrow and wide goals (Fig. 5*B*). Across the population of muscle samples for monkey M, 75% of samples had significantly greater activities for unperturbed reaches to the narrow goal than the wide goal in the movement epoch (movement epoch, 200 ms before until 20 mms after faux-jump onset; Fig. 5*A*,*B*, gray region; two-sample t test between goal shapes, $p < 0.01$) with the average activity for the narrow goal being 15% greater than the activity for the wide goal (Fig. 5*C*, significant muscles are black filled circles). In contrast, there were no significant differences in activities for the narrow and wide goal in activity recorded from monkey C (Fig. 5*C*, gray open circles).

The magnitudes of the muscle activities were highly correlated between the narrow and wide goals (Pearson's correlation coefficient $r = 0.99$, all muscles included from monkeys M and C). Furthermore, there was a strong temporal correlation between muscle activities for the narrow and wide goal reaches with a median correlation coefficient of 0.80 across muscles, which was significant (shuffle $r = 0.16$, $p < 0.001$;

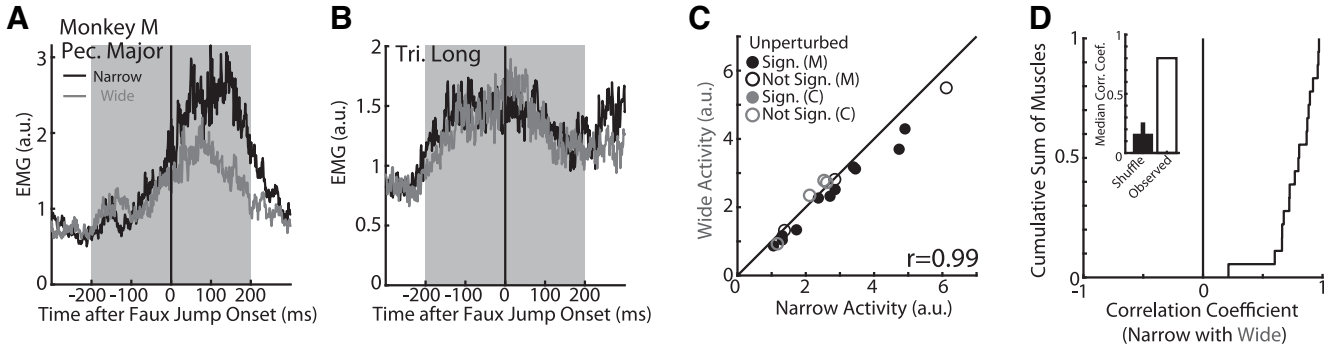

Figure 5. Muscle activity during unperturbed reaches to the narrow and wide goals for the cursor-jump variant of task. ***A***, Average activity of the pectoralis major muscle for reaches to the narrow and wide goals. Activities are aligned to faux jump onset. ***B***, Same as ***A*** for the long head of the triceps. ***C***, Comparison of the mean narrow and wide goal activities across muscles inside the 400 ms epoch centered on the faux jump onset; *r* indicates Pearson's correlation coefficient. Monkeys M and C are denoted by the black and gray markers, respectively, and reflect averages pooled across multiple sessions (see above, Results, Experiment 1: goal redundancy and feedback responses to cursor jumps; number of trials, monkey M = 95, monkey C range 45–153). Filled circles denote muscles with significantly different activities for the narrow and wide goals. ***D***, Cumulative sum of the temporal correlation coefficients between the narrow and wide goal activities across muscles (monkeys M and C pooled). Same 400 ms epoch as ***C***. Inset, The median correlation coefficient from the shuffled distribution (mean ± SD) and the observed median coefficient. Recorded from monkey M using indwelling EMG with 95 unperturbed trials for each goal shape (***A***, ***B***).

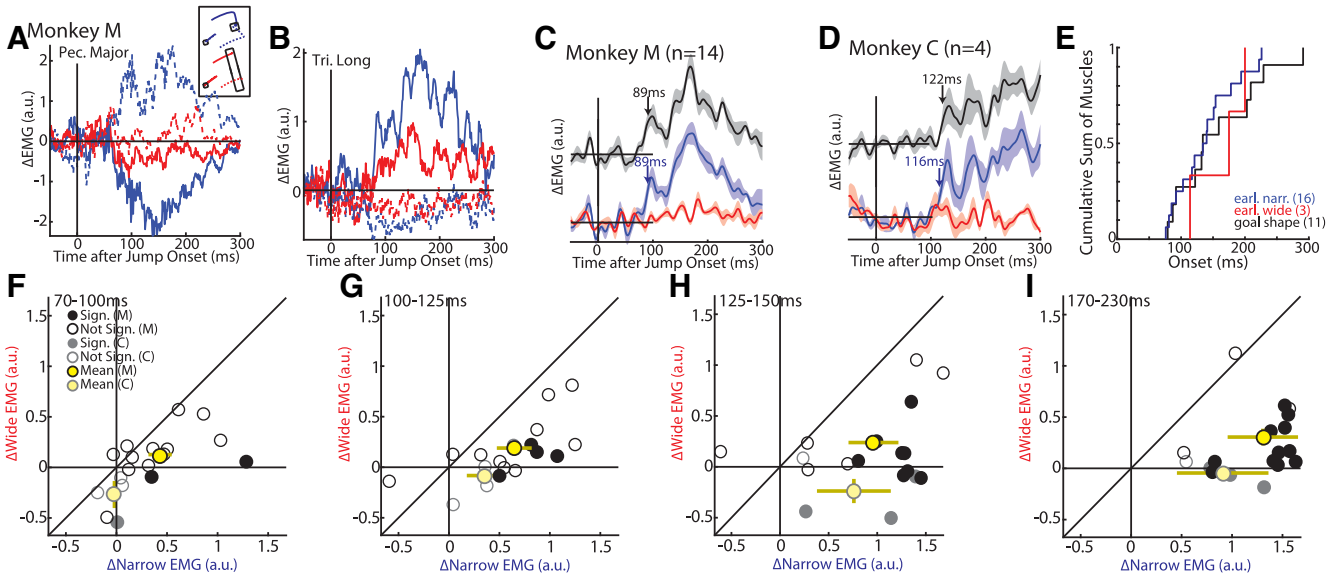

Figure 6. Muscle activity in response to the cursor jumps. ***A***, The change in activity for the pectoralis major muscle in response to the cursor jumps when reaching for the narrow and wide goals. ***B***, Same as ***A*** for the long head of the triceps. ***C***, Group average change in muscle activity to the cursor jumps for the narrow (bottom, blue) and wide goals (bottom, red). Top, The resulting difference signal between the activities for the narrow and wide goals is shown in the black trace. Muscle activities were averaged across their preferred directions for all jump-sensitive muscles. Blue and black arrows denote when a significant increase in activity from baseline started for the narrow goal reaches and difference signal, respectively. No onset was detected for the wide goal reaches. Average across 14 muscle samples with 31 perturbation trials per goal shape. ***D***, Same as ***C*** for monkey C. Average across four muscles with number of trials per goal shape ranging across muscles from 15 to 51. ***E***, Onsets for individual muscles presented as a cumulative sum. Numbers in brackets reflect the number of muscle samples with a detectable onset. Muscles recorded from monkeys M and C pooled. ***F***, Comparison between the absolute change in muscle activities for the narrow and wide goals in the 70–100 ms epoch. Muscles recorded from monkeys M and C are denoted in the black and gray markers, respectively. Yellow circles and bars denote the means and SDs for each monkey. Filled circles denote muscle samples that had significantly different activities for the narrow and wide goals. ***G–I***, same as ***F*** except for the 100–125 ms (***G***), 125–150 ms (***H***), and 170–230 ms (***I***) epochs. Recorded from monkey M using indwelling EMG with 30 perturbation trials for each perturbation direction and goal shape (***A***, ***B***).

Fig. 5*D*). Thus, muscle activity was largely similar between unperturbed reaches to the narrow and wide goals with a slight bias toward greater activity for reaches to the narrow goal for monkey M.

Figure 6, *A* and *B*, shows the change in activities (ΔEMG) for PM and TLong for cursor-jump trials (monkey M, unperturbed activity subtracted off). For both muscles, activity started to differentiate between jump directions starting in <100 ms. Activity also appeared to differentiate based on goal shape starting ~100 ms after the jump with greater change in activity for the narrow goal than the wide goal. We normalized each muscle sample by its perturbation response (0–300 ms after perturbation) and identified the preferred direction by the direction with the largest evoked response in the perturbation epoch for the narrow goal (0–300 ms after perturbation onset). Muscle activities across muscle samples were averaged to construct a population signal (Fig. 6*C*). We found the population signal increased from baseline for the narrow goal starting ~89 ms after the cursor jump (Fig. 6*C*, bottom). However, we were unable to detect an onset for the wide goal reflecting the absence of corrective muscle activity for the cursor jump. The population response differentiated based on the goal shape almost

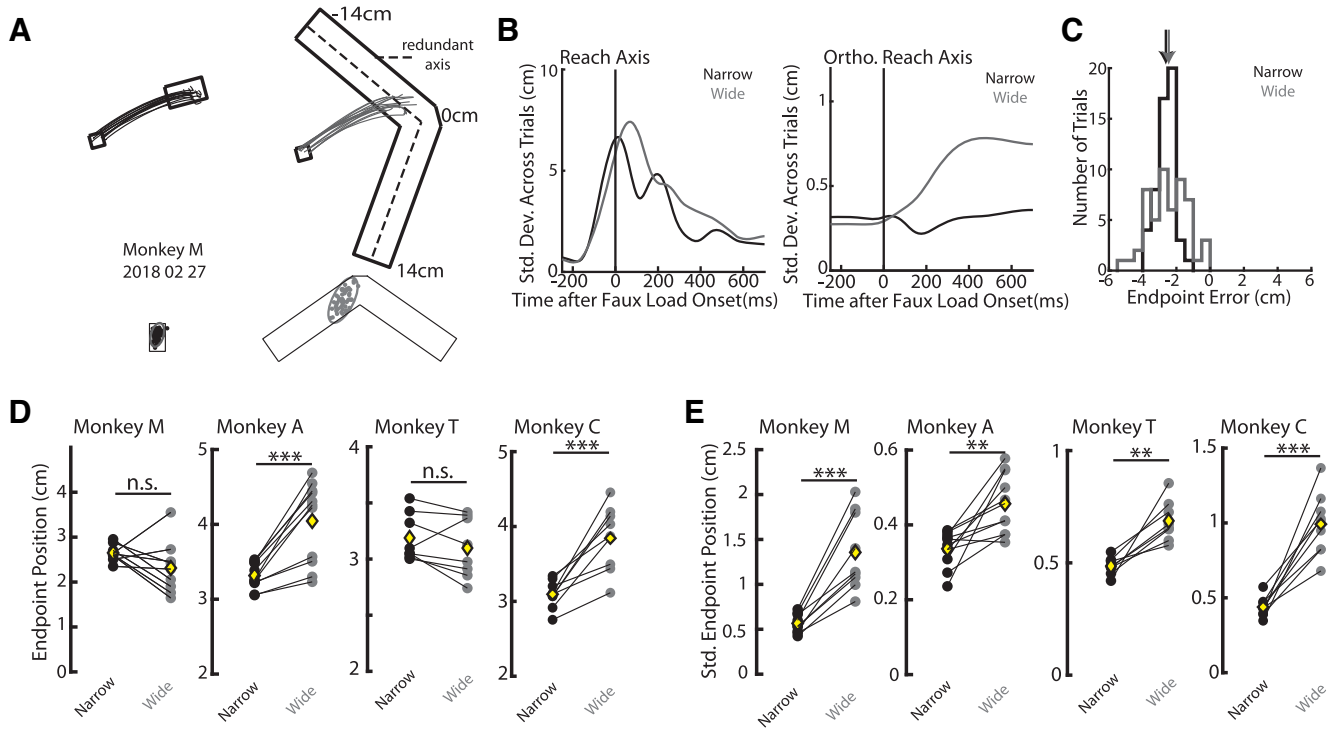

Figure 7. Example kinematics for unperturbed trials for the mechanical-load variant of task. ***A***, Hand paths from one session for monkey M to the narrow (left) and wide (right) goals. Dashed line on the wide goal denotes the redundant axis. ***B***, SDs of the hand position across trials for the narrow and wide goal reaches. ***C***, Reach endpoint histograms for reaches to the narrow and wide goals from the same session as ***A***. Zero denotes the middle of the redundant axis (***A***, middle of dashed line). Arrows denote the means of the distributions. ***D***, The mean endpoint positions for the narrow and wide goals across all recording sessions from both monkeys. Yellow diamonds denote the means across sessions. ***E***, Same as ***D*** for SDs of the endpoint positions. $^{**}p < 0.01$, $^{***}p < 0.001$. From the same recording session with 50 unperturbed trials each for the narrow and wide goal (***A–C***).

immediately with an onset detected at 89 ms (Fig. 6*C*, top). Similar results were found with monkey C, except that the population signals started to differentiate from baseline (116 ms; Fig. 6*D*, bottom) and between goal shapes (122 ms; Fig. 6*D*, top) later, which may be because of the noisier nature of surface EMG. Similar trends were found when analyzing onsets of individual muscles (Fig. 6*E*).

Next, we compared the response of each muscle in its preferred direction for the narrow and wide goals in the epochs of 70–100, 100–125, 125–150, and 170–230 ms (Fig. 6*F–I*). For each muscle we applied a two-way ANOVA with time (levels, four epochs) and goal shape (levels, narrow and wide) as factors and found 89% of samples had a significant interaction effect between time and goal shape ($p < 0.05$, Bonferroni correction factor of 2). *Post hoc* two-sample *t* tests revealed 17, 27, 61, and 78% of samples had significantly different muscle responses in the 70–100, 100–125, 125–150, and 170–230 ms epochs, respectively ($p < 0.05$, Bonferroni correction factor 4; Fig. 6*F–I*, filled circles). Note, similar results were found when using nonparametric *post hoc* tests (rank sum test, percentage of samples that were significant in each epoch, 11, 17, 50, and 72%) On average, the activity for the wide goal was 88, 78, 86, and 81% smaller than the activity for the narrow goal in the 70–100, 100–125, 125–150, and 170–230 ms epochs, respectively. We examined group-level responses across trial-averaged muscle responses by applying a two-way repeated-measures ANOVA with time (levels, four epochs) and goal shape (levels, narrow and wide) as factors. We found a significant main effect of goal shape ($F_{(1,17)} = 58.1$, $p < 0.001$) and an interaction between goal shape and time ($F_{(3,51)} = 17.9$, $p < 0.001$). *Post hoc* paired *t* tests confirmed that responses for the narrow goal were significantly greater than for the wide goal in all epochs (70–100, 100–125, 125–150, 170–230 ms, df =17, all epochs, $t_{(11)} = 3.8$, $t_{(11)} = 5.58$, $t_{(11)} = 5.37$, $t_{(11)} = 9.8$, $p < 0.005$, $p = 0.001$, $p < 0.001$, $p < 0.001$, Bonferroni correction factor 4). Similar results were found with nonparametric *post hoc* tests (signed rank test, probability value in each epoch, $p = 0.005$, $p = 0.004$, $p = 0.005$, $p < 0.001$). Collectively, these results indicate muscle activity in response to visual feedback of the limb differentiates based on goal shape within ~90–120 ms.

Experiment 2: goal redundancy and feedback responses to mechanical loads

We modified the above reaching task to probe feedback responses to mechanical loads. We increased the size of the redundant dimension of the goal to better differentiate corrections to the narrow and wide goals (Fig. 1*B*). We also adopted a shape for the wide goal that was similar to an arrowhead so that edges of the goal were in closer proximity to the monkey, thus making it easier to reach on perturbation trials. For monkeys M, A, T, and C, we recorded 10, 11, 8, and 9 behavioral sessions of the animals performing the task on separate days. Again, monkeys were able to perform the task with high efficiency (success rates across all trials monkeys M, A, T, C, narrow targets = 96, 95, 95, 96%; wide targets = 97, 100, 97, 91%).

Figure 7*A* shows the hand paths for monkey M to the narrow (left) and wide (right) goals from one recording session. Similar to the previous task, there was more variability in the reaches to the wide goal (Fig. 7*B*,*C*). Across sessions we found no significant different in endpoint position for monkeys M and T, whereas there was a 0.7 cm change in endpoint positions for monkeys A ($t_{(10)} = 6.1$, $p < 0.001$) and C ($t_{(8)} = 5.8$, $p < 0.001$). The variability of reach endpoints were 2.2, 1.4, 1.4, and 2.3 times greater for

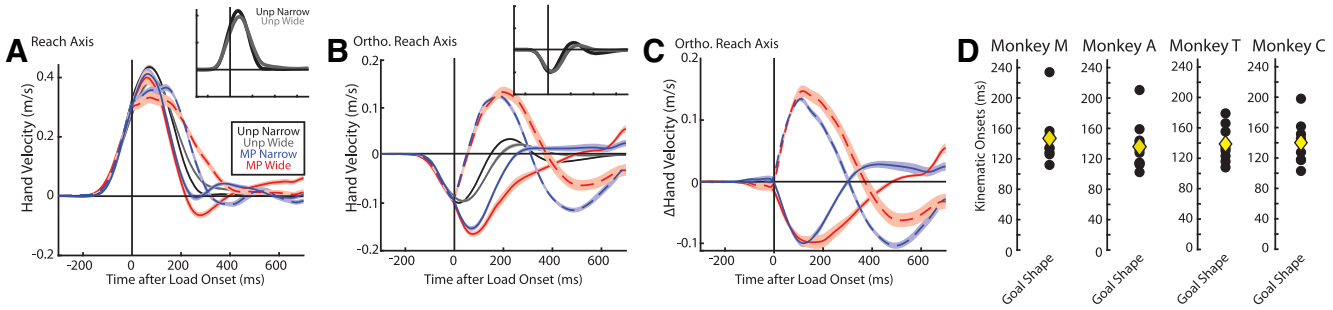

Figure 8. Example hand velocity profiles for the mechanical-load variant of task. ***A***, The hand velocity along the reach axis for the narrow and wide goals. Velocity was aligned to the load onset. Inset, The unperturbed reaches to the narrow and wide goals. Unp Narrow and Unp Wide, Unperturbed reaches to the narrow and wide goals, respectively. MP Narrow and MP Wide, Mechanical load trials for reaches to the narrow and wide goals, respectively. Solid and dashed lines denote mechanical loads away from the body and toward the body, respectively. ***B***, Same as ***A*** for the hand velocity along the orthogonal reach axis. ***C***, The change in the hand velocity on mechanical-load trials for the narrow and wide goals. ***D***, Time when corrections differentiated based on goal shape across sessions. Yellow diamonds are the means across sessions. From the same recording session as Figure 7, *A–C*, with 13 perturbed trials for each perturbation direction and goal shape and 50 unperturbed trials for each goal shape (***A–C***).

the wide goal than for the narrow goal for monkeys M, A, T, C, respectively (Fig. 7*E*; paired *t* test, monkeys M and A, $t_{(9)} = 5.3$, $t_{(10)} = 4.1$, $t_{(7)} = 5.2$, $t_{(8)} = 7.3$, $p < 0.001$, $p = 0.002$, $p = 0.001$, $p < 0.001$).

Figure 8, *A* and *B* (insets), show the unperturbed hand velocities during the same recording session along the reach and orthogonal reach axes, respectively. In contrast to experiment 1, there was a small decrease in the peak hand velocity in both directions for the wide goal compared with the narrow goal. The hand speed was not significantly different for monkeys M (narrow 0.45 m/s, wide 0.44 m/s, paired *t* test, $t_{(9)} = 1.5$, $p = 0.2$) and T (narrow 0.38 m/s, wide 0.36 m/s, $t_{(7)} = 2.3$ $p = 0.05$); however, there was a significant reduction for the wide goal for monkey A (narrow 0.52 m/s, wide 0.47 m/s, $t_{(10)} = 8.0$, $p < 0.001$) and a significant increase for the wide goal for monkey C (narrow 0.36 m/s, wide 0.38 m/s, $t_{(8)} = 2.6$, $p = 0.03$).

Next, we examined how goal redundancy affected corrective responses for the unexpected mechanical loads. Figure 9*A* shows hand paths of monkey M on mechanical-load trials. There is a clear correction present when the monkey was reaching for the narrow goal, which again had little overshooting or undershooting of the goal. In contrast, when reaching for the wide goal, monkeys exhibited greater variability and corrected less for the mechanical loads (Fig. 9*B*,*C*). Across sessions, there was a greater change in reach endpoints (change relative to unperturbed trials) for the wide goal than the narrow goal (Fig. 9*D*,*F*; paired *t* tests, mechanical loads away from/toward body, monkey M, $t_{(9)} = 7.8$, $t_{(9)} = 4.9$; monkey A, $t_{(10)} = 9.5$, $t_{(10)} = 20$; monkey T, $t_{(7)} = 3.6$, $t_{(7)} = 7.6$; monkey C, $t_{(8)} = 6.1$, $t_{(8)} = 11.7$, $p < 0.01$ for all comparisons, Bonferroni correction factor 2). There was also greater variability in the reach endpoints on perturbation trials in both directions (Fig. 9*E*,*G*; monkey M, $t_{(9)} = 8.3$, $t_{(9)} = 3.0$, $p < 0.001$, $p = 0.02$; monkey A, $t_{(10)} = 5.4$, $t_{(10)} = 4.5$, $p < 0.001$, $p = 0.004$; monkey T, $t_{(7)} = 4.8$, $t_{(7)} = 5.4$, $p = 0.004$, $p = 0.002$; monkey C, $t_{(8)} = 4.9$, $t_{(8)} = 4.4$, $p = 0.002$, $p = 0.004$, Bonferroni correction factor 2).

For the mechanical-load trials, kinematic changes were primarily in the orthogonal reach axis although changes could also be detected in the reach axis (Fig. 8*A*,*B*). Detecting the earliest kinematic correction to a mechanical load is difficult as the limb is already moving because of the momentum from the load (Fig. 8*C*). However, we could detect differences in corrections based on goal shape that started at 147, 136, 139, and 140 ms for monkeys M, A, T, C, respectively (Fig. 8*D*).

For muscle activity recorded from monkey M (indwelling), we pooled recordings over the course of eight behavioral sessions as the differences in the corrective responses were comparatively weaker than for the cursor perturbations. All muscle samples from monkey M were included as they all showed perturbation-related activity. For monkey C, we again recorded using surface electrodes over the course of seven recordings sessions and kept six, four, three, and six recording sessions for TLat, Br, Bi, and TLong, respectively.

Figure 10, *A* and *B*, shows the average muscle activity on unperturbed trials for PM and TLong aligned to the faux-load onset (monkey M). Both muscles had similar temporal structure for the goal shapes, however, for PM there was greater activity for the narrow goal than the wide goal. Across muscle samples, all samples from monkey M had significantly greater activities for unperturbed reaches to the narrow goal than the wide goal in the movement epoch (two-sample *t* test, $p < 0.01$) with the average activity for the wide goal being 17% smaller than the activity for the narrow goal (Fig. 10*C*, significant muscles are filled black circles). In contrast, no muscle samples collected from monkey C were significantly different between the narrow and wide goals (gray circles). The muscle activity magnitudes were highly correlated between the two goal shapes for both monkeys (Pearson's correlation coefficient across all muscles, $r = 0.98$), and there were was a strong temporal correlation between activities for the narrow and wide goals (Fig. 10*D*, median $r = 0.891$), and the distribution across muscles was shifted more to the right than the shuffled distribution (Fig. 10*D*, inset, $r = 0.49$, $p < 0.001$).

Changes in muscle activity in response to the mechanical loads started within ~20–50 ms of an applied load (Fig. 11*A–E*, averages constructed across all load-sensitive muscles). For monkey M, the population activity across load-sensitive muscles increased from baseline starting at 62 and 64 ms for the narrow and wide goals, respectively (Fig. 11*C*, normalized by perturbation response). For monkey C, activity increased from baseline earlier at 33 and 26 ms for the narrow and wide goals, respectively (Fig. 11*D*). Activity differentiated based on goal shape starting at 78 and 106 ms for monkeys M and C, respectively (Fig. 11*C–E*).

Next, we compared the response of each muscle in the epochs of 20–50, 50–75, 75–100, and 120–180 ms (Fig. 11*F–I*). A two-way ANOVA with time and goal shape as factors found 85% of muscle samples had a significant interaction effect. *Post hoc* two-sample *t* tests revealed 6, 17, 47, and 94% of samples had significantly different muscle responses in the 20–50, 50–75, 75–100,

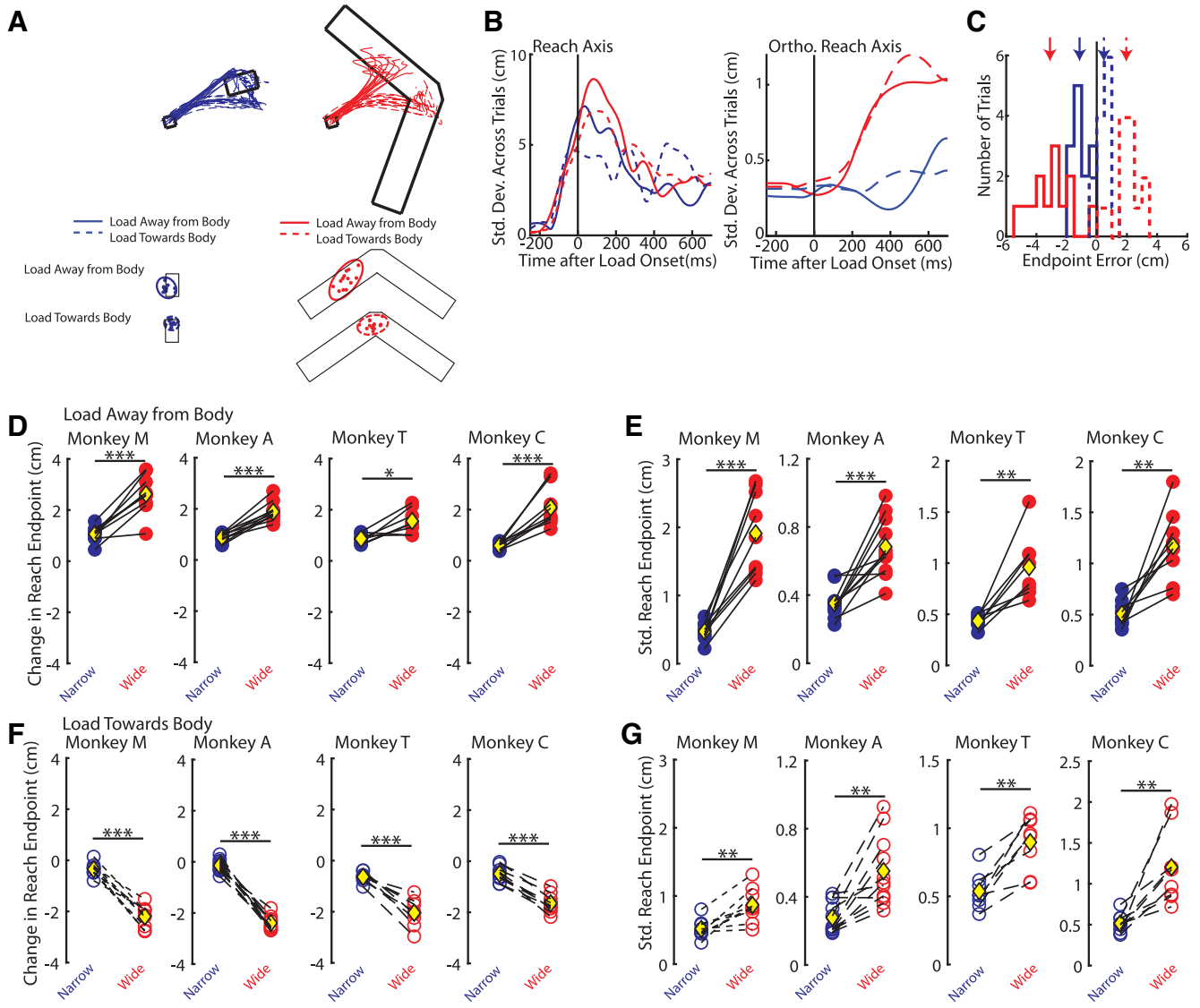

Figure 9. Example kinematics on mechanical-load variant of task. ***A***, Top, Hand paths from monkey M for mechanical-load trials. Bottom, Reach endpoints and the 95% confidence ellipse. Solid and dashed lines denote mechanical loads away from the body and toward the body, respectively. ***B***, SDs of the hand position across trials for the narrow and wide goal reaches. ***C***, The change in reach endpoint histograms (change relative to unperturbed reach trials). Zero denotes the mean of the reach endpoints on unperturbed trials (Fig. 7*C*, arrows). Arrows denote the means of the distributions. ***D***, The mean change in reach endpoints for loads away from the body across all recording sessions. ***E***, Same as ***D*** for the SD in reach endpoints. ***F***, ***G***, Same as ***D***, ***E*** for loads toward the body. $^{**}p < 0.01$, $^{***}p < 0.001$. From same recording session as Figure 7, *A–C*, with 13 perturbed trials for each perturbation direction and goal shape (***A–C***).

and 120–180 ms epochs, respectively ($p < 0.05$, Bonferroni correction factor 4; Fig. 11*F–I*, filled circles;). Similar results were found when using nonparametric *post hoc* tests (rank sum test, percentage of samples that were significant in each epoch, 6, 25, 44, and 100%) On average, the activity for the wide goal was 13, 12, 39, and 43% smaller than the activity for the narrow goal in the 20–50, 50–75, 75–100, and 120–180 ms epochs, respectively. We applied a two-way repeated-measures ANOVA with time (levels, four epochs) and goal shape (levels, narrow and wide) to the trial-averaged muscle responses. We found a significant main effect of goal shape ($F_{(1,19)} = 22.3$, $p < 0.001$) and an interaction between goal shape and time ($F_{(3,57)} = 17.8$, $p < 0.001$). *Post hoc* paired *t* tests confirmed that responses for the narrow goal were significantly greater than for the wide goal in the 75–100 ms ($t_{(19)} = 3.2$, $p = 0.017$) and 120–180 ms ($t_{(19)} = 7.0$, $p < 0.001$; Bonferroni correction factor 4) epochs, but not significantly different in the earlier epochs (20–50 ms, $t_{(19)} = 0.3$ $p = 1$; 50–75 ms, $t_{(19)} = 0.5$, $p = 1$). Similar results were found with nonparametric *post hoc* tests (signed rank test, probability value in each epoch, $p = 0.98$, $p = 1$, $p = 0.026$, $p < 0.001$).

Discussion

Exploiting redundancies is an important feature of many motor control theories including OFC (Bernstein, 1967; Scholz et al., 2000; Todorov and Jordan, 2002; Latash, 2012) and its variations including time-to-target (Oostwoud Wijdenes et al., 2011; Česonis and Franklin, 2020) and robust control (Cluff et al., 2019; Crevecoeur et al., 2019; Bian et al., 2020). Studies demonstrate how humans are capable of exploiting redundancies during motor actions (Todorov and Jordan, 2002; Diedrichsen, 2007; Mutha and Sainburg, 2009; Knill et al., 2011; Dimitriou et al., 2012; Nashed et al., 2012, 2014; Cluff and Scott, 2015). Here, we demonstrate that monkeys exploit the spatial redundancy of a goal with performance similar to humans. Monkeys exhibited

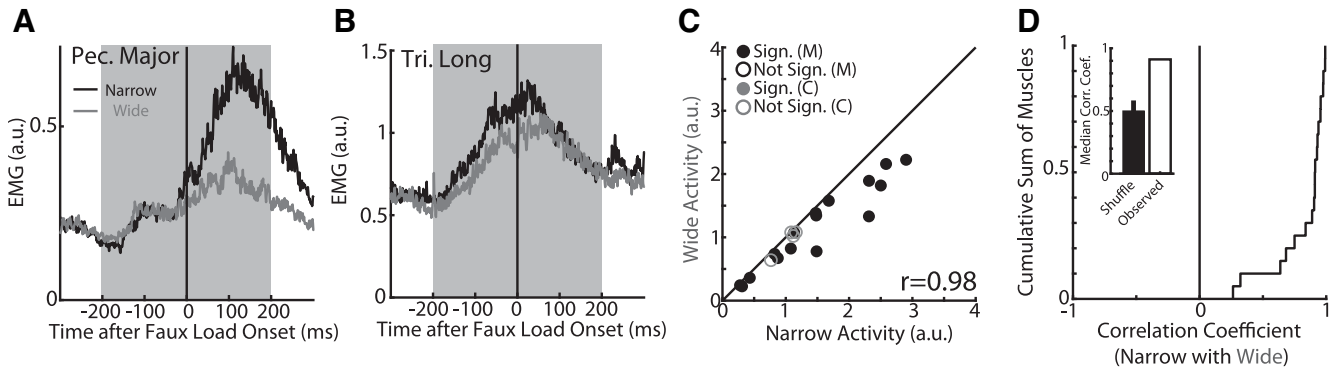

Figure 10. Muscle activity during unperturbed reaches to the narrow and wide goals for the mechanical-load variant of task. ***A***, Average activity of the pectoralis major muscle for reaches to the narrow and wide goals. Activity are aligned to faux-load onset. ***B***, Same as ***A*** for the long head of the triceps. ***C***, Comparison of the mean narrow and wide goal activities across muscles inside the 400 ms epoch centered on the faux-load onset; r indicates Pearson's correlation coefficient. Monkeys M and C are denoted by the black and gray markers. Number of trials, monkey M = 363, monkey C range of 156–383. Filled circles denote muscles with significantly different activities for the narrow and wide goals. ***D***, Cumulative sum of the temporal correlation coefficients between the narrow and wide goal activities across muscles (muscles from monkeys M and C pooled). Same 400 ms epoch as ***C***. Inset, The median correlation coefficient from the shuffled distribution (mean ± SD) and the observed median coefficient. Recorded from monkey M using indwelling EMG with 360 unperturbed trials for each goal shape (***A***, ***B***).

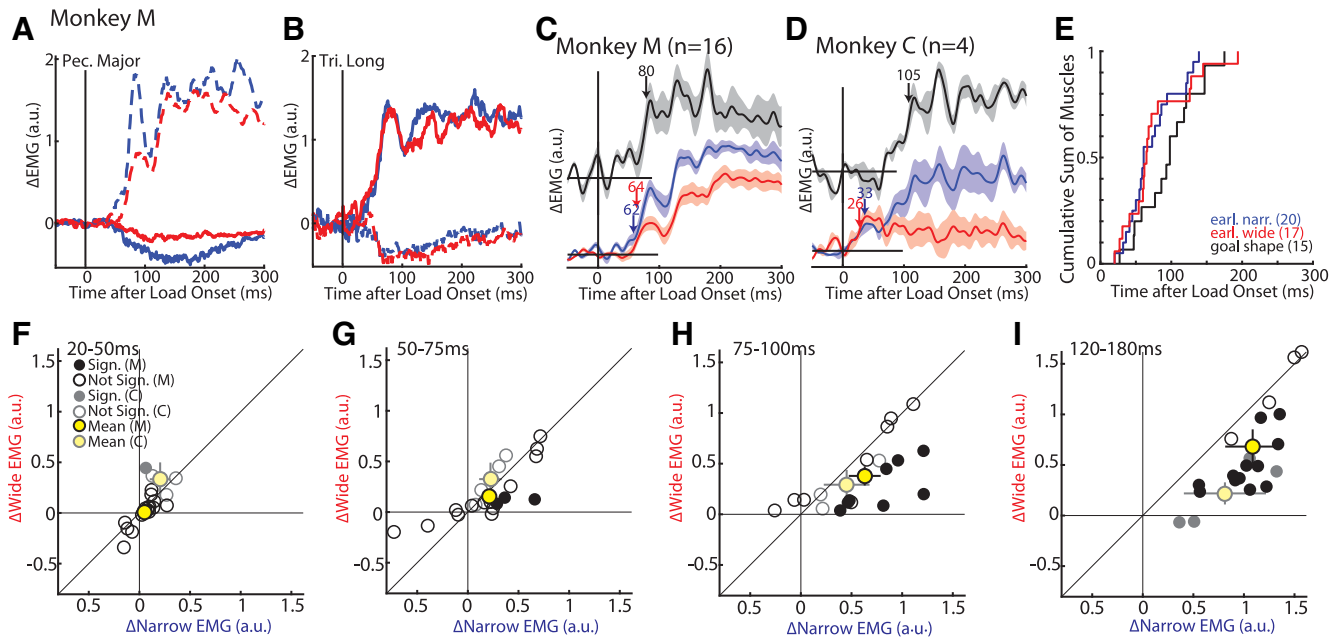

Figure 11. Muscle activity in response to the mechanical loads. ***A***, The change in activity for the pectoralis major muscle in response to the mechanical loads when reaching for the narrow and wide goals. Same session as in Figure 10. ***B***, Same as ***A*** for the long head of the triceps. ***C***, Group average change in muscle activity for the mechanical loads for the narrow (bottom, blue) and wide goals (bottom, red). All load-sensitive muscle samples were included. Top, The resulting difference signal between the activities for the narrow and wide goals is shown in the black trace. Muscle activities were averaged across their preferred directions. Blue and red arrows denote when a significant increase in activity from baseline (500 ms before mechanical load onset) started for the narrow and wide goal reaches, respectively. Black arrow denotes when a significant increase in activity from baseline started for the difference signal. Averaged across 16 muscle samples with 90 perturbation trials for each goal shape. ***D***, Same as ***C*** for monkey C. Average across four muscles with number of trials per goal shape ranging across muscles from 36 to 89. ***E***, Onsets for individual muscles presented as a cumulative sum. Numbers in brackets reflect the number of muscle samples with a detectable onset. Muscles from monkeys M and C were pooled. ***F***, Comparison between the absolute change in muscle activities for the narrow and wide goals in the 20–50 ms epoch. Muscles recorded from monkeys M and C are denoted in the black and gray markers. Yellow circles and grey bars denote the mean and SD for each monkey. Filled circles denote muscle samples that had significantly different activities for the narrow and wide goals. ***G–I***, same as ***F*** except for the 50–75 ms (***G***), 75–100 ms (***H***), and 120–180 ms (***I***) epochs. Recorded from monkey M using indwelling EMG with 90 perturbation trials for each perturbation direction and goal shape (***A***, ***B***).

greater variability in their reach endpoints when reaching to a more spatially redundant goal. Rapid corrective responses to limb perturbations were also attenuated to exploit goal redundancy with observable changes in muscle activity starting in <100 ms.

Although it is impossible to know for certain whether the monkeys recognized that they could reach anywhere on the wide target, there are several lines of evidence that indicate monkeys exploited goal redundancy similar to humans and OFC models. First, OFC predicts that trial-by-trial variability even on unperturbed trials should be larger for goals with greater spatial redundancy with variability constrained along the redundant axis of the goal (Knill et al., 2011; Nashed et al., 2012). Previous studies in humans (Knill et al., 2011; Nashed et al., 2012; Cross et al., 2019) and the current study in monkeys demonstrate similar OFC-like structure with variability growing throughout the duration of the reach and culminating in greater variability in the reach endpoints along the redundant axis of the goal.

Second, OFC predicts that corrections to external perturbations should be smaller for more spatially redundant goals provided the perturbations are along the redundant axis, which is a feature observed in human corrections to visual and mechanical perturbations (Knill et al., 2011; Nashed et al., 2012; Cross et al., 2019). Here, we demonstrated monkeys also show smaller corrective responses when reaching for the wide goal. This was evident for the wide goal as a 2–4 cm shift in the reach endpoints on perturbation trials from where monkeys were reaching on unperturbed trials. In contrast, there was <1 cm shift in endpoints when monkeys were reaching for the narrow goal on perturbation trials. Endpoints on perturbation trials were also more variable when reaching for the wide goal, indicating monkeys did not simply learn to reach for a particular goal location on perturbation trials. Collectively, these results argue that monkeys understood goal redundancy and did not simply learn an arbitrary mapping between sensory stimuli and behavioral response that mimicked the expected behavior.

Monkeys also generated muscle activity patterns to the mechanical loads that were similar to OFC models and humans. OFC models predict an initial increase in control output in response to the mechanical load regardless of goal shape reflecting that the controller must counteract the external load to stabilize the limb (Nashed et al., 2012). Control output differentiates based on goal shape later with greater activity for the narrow goal to generate the necessary kinematic correction. Muscle activity evoked by the mechanical loads exhibit similar patterns as the control output with an initial increase starting at ~50 ms regardless of target shape, reflecting a need to stabilize the limb in response to the mechanical load. As a result, muscle activity differentiating based on goal shape emerged later starting at ~70 ms in both humans (Nashed et al., 2012) and monkeys (present study). Other studies have also found humans and monkeys exhibit similar timing for when corrective responses to mechanical loads are modulated by different contexts including for limb physics (Kurtzer et al., 2008; Pruszynski et al., 2011), task instruction (Hammond, 1956; Evarts and Tanji, 1976; Pruszynski et al., 2008, 2014; Omrani et al., 2014), and adaptation (Cluff and Scott, 2013; Maeda et al., 2018, 2020), which all start 60–70 ms after the onset of the load. More broadly, rhesus monkeys also exhibit similar voluntary reaction times to a visual target as humans (200–300 ms; Georgopoulos et al., 1981; Churchland and Shenoy, 2007), which highlights how monkeys are a useful model to investigate the neural circuits that underlie voluntary control and flexible feedback processing during motor actions.

Our results contrast with previous findings by Bizzi et al. (1982, 1984), who found monkeys correct back to the original trajectory when encountering an assistive mechanical load. One possible reason is that monkeys may have learned an implicit timing constraint for when the arm should arrive at the goal and thus resisted the applied load to prevent arriving too early. Indeed, humans also show similar corrections but only when given a timing constraint (Cluff and Scott, 2015).

It is important to note that monkeys displayed the behavioral effect of goal shape to various degrees as some monkeys were more strongly affected by the goal shape (monkeys M and C) than other monkeys (monkeys A and T), particularly for the unperturbed reaches. This variability may reflect our paradigm as we adopted a largely single-joint reaching movement for unperturbed trials in contrast to human studies that used a multijoint reach (Nashed et al., 2012; de Brouwer et al., 2017; Cross et al., 2019). However, it is unclear how much variability exists across human participants as previous studies have largely examined group-level effects, whereas the present study examined effects within each monkey. Nonetheless, our paradigm still produced behavioral effects in monkeys that exhibited similar qualities as human performance.

One limitation we found was that muscle activity was greater in amplitude for unperturbed reaches to the narrow goal than the wide goal, particularly for monkey M. Presumably, this increased activity was also present on mechanical-load trials and poses a potential problem for interpreting onsets to mechanical loads because of a gain-scaling effect, where muscle activity evoked by a load scales with the size of the background muscle activity (Marsden et al., 1976; Bedingham and Tatton, 1984; Matthews, 1986; Stein et al., 1995; Pruszynski et al., 2009). Thus, greater muscle activity for the narrow goal following a mechanical load could simply reflect a gain-scaling effect. However, we believe this is unlikely as the effect of gain scaling typically only influences muscle activity within 20–50 ms after an applied load (Pruszynski et al., 2009; Nashed et al., 2012), whereas in our study activity differentiated based on goal shape at ~70 ms. Second, we did not detect a significant difference in muscle activity for monkey C on unperturbed trials using surface electrodes and still found similar muscle timing.

Our results highlight that monkeys exhibit corrective responses that exploit goal redundancy that is similar to humans and thus provides an important model for addressing questions concerning how flexible feedback responses are generated by neural circuits. Studies highlight that primary motor cortex (M1) is involved with generating flexible muscle responses to sensory feedback. M1 receives rich proprioceptive feedback with responses that start within ~20 ms of an applied load (Conrad et al., 1974, 1975; Wolpaw, 1980; Fromm et al., 1984; Bauswein et al., 1991; Picard and Smith, 1992; Herter et al., 2009; Takei et al., 2018; Heming et al., 2019; Cross et al., 2020, 2021). Importantly, proprioceptive feedback responses in M1 are modulated by several behavioral factors including limb physics (Pruszynski et al., 2011), prior instruction (Evarts and Tanji, 1976; Pruszynski et al., 2014), and task engagement (Omrani et al., 2014) within 50 ms of an applied load. The flexible responses in M1 preceded the corresponding change in muscle activity by ~10 ms, consistent with the conduction delay between M1 and the periphery (Cheney and Fetz, 1984; Lemon et al., 1986). Thus, if M1 is involved with generating proprioceptive feedback responses that exploit goal redundancy than M1 activity reflecting goal redundancy should emerge ~60 ms after the load onset.

However, it is likely that other brain areas also contribute to generating muscle responses that exploit goal redundancy. Premotor cortex, somatosensory cortex, parietal area 5, and the cerebellum all project to M1 (Jones et al., 1978; Porter and Lemon, 1993; Dea et al., 2016) and rapidly respond to proprioceptive feedback within <70 ms with activity patterns that are context dependent (Wolpaw, 1980; Lamarre et al., 1983; Strick, 1983; Chapman et al., 1984; Pruszynski et al., 2011, 2014; London and Miller, 2013; Omrani et al., 2014, 2016). However, context is not homogenously shared across these areas as premotor cortex, M1, and cerebellum exhibit activity patterns consistent with implementing a control policy, whereas somatosensory and parietal areas exhibit patterns of activity consistent with state estimation (Strick, 1983; Omrani et al., 2016). These results are also supported by a recent study examining temporary inactivation of a subset of these areas (Takei et al., 2021). Thus, given that goal

redundancy is a property of the control policy, we predict context-dependent responses will emerge first in premotor cortex, M1, and the cerebellum.

Monkeys also generated muscle activity patterns to the cursor jumps that were similar to those of humans and OFC models. Unlike mechanical loads, cursor jumps do not require the controller to counteract an external load as the disturbance is only a kinematic error. Thus, control output of the OFC model should be unaffected by the cursor jump when reaching for the wide goal. Similarly, muscle activity of humans (Cross et al., 2019) and monkeys is largely unchanged by a cursor jump when reaching to a wide goal resulting in activity that differentiates based on goal redundancy ~90 ms after a cursor jump. This differentiation is also unlikely because of a gain-scaling effect as background muscle activity does not appear to affect correction strength for visual perturbations (Franklin et al., 2017).

It is less clear how visual feedback is processed by frontoparietal circuits and how behavioral context influences visual processing in these areas. A common assumption is that visual feedback is processed by posterior parietal cortex, which is then sent toward frontal circuits including M1 and premotor cortex (Goodale and Milner, 1992; Desmurget et al., 1999; Pisella et al., 2000; Gaveau et al., 2014). Thus, consistent with OFC, visual feedback is processed initially by circuits involved with state estimation followed by circuits involved with implementing the control policy. However, there is evidence that visual feedback responses arrive first in premotor cortex (50–70 ms) followed by M1 (70–100 ms) and finally parietal area 5 (Cisek and Kalaska, 2005; Archambault et al., 2011; Ames et al., 2014; Stavisky et al., 2017; Cross et al., 2021). Thus, premotor cortex may generate the earliest muscle response to visual feedback rather than M1.

Alternatively the superior colliculus may be involved with generating rapid motor responses to visual feedback (Alstermark et al., 1987; Day and Brown, 2001; Pruszynski et al., 2010; Corneil and Munoz, 2014; Day, 2014; Cross et al., 2019; Kozak et al., 2019). Activity in the superior colliculus correlates with muscle activity of the upper arm during reaching (Werner, 1993; Werner et al., 1997; Stuphorn et al., 1999), and stimulation of the superior colliculus can evoke reaching-like behavior (Philipp and Hoffmann, 2014). Further investigations are needed to elucidate the underlying neural circuits involved with generating rapid visual responses for which our behavioral task could be invaluable.

References

Alstermark B, Górska T, Lundberg A, Pettersson L-G, Walkowska M (1987) Effect of different spinal cord lesions on visually guided switching of target-reaching in cats. Neurosci Res 5:63–67.

Ames KC, Ryu SI, Shenoy KV (2014) Neural dynamics of reaching following incorrect or absent motor preparation. Neuron 81:438–451.

Archambault PS, Ferrari-Toniolo S, Battaglia-Mayer A (2011) Online control of hand trajectory and evolution of motor intention in the parietofrontal system. J Neurosci 31:742–752.

Bauswein E, Fromm C, Werner W, Ziemann U (1991) Phasic and tonic responses of premotor and primary motor cortex neurons to torque changes. Exp Brain Res 86:303–310.

Bedingham W, Tatton WG (1984) Dependence of EMG responses evoked by imposed wrist displacements on pre-existing activity in the stretched muscles. Can J Neurol Sci 11:272–280.

Bernstein N (1967) The co-ordination and regulation of movements. Oxford, UK: Pergamon.

Bian T, Wolpert DM, Jiang Z-P (2020) Model-free robust optimal feedback mechanisms of biological motor control. Neural Comput 32:562–595.

Bizzi E, Accornero N, Chapple W, Hogan N (1982) Arm trajectory formation in monkeys. Exp Brain Res 46:139–143.

Bizzi E, Accornero N, Chapple W, Hogan N (1984) Posture control and trajectory formation during arm movement. J Neurosci 4:2738–2744.

Bonnet M (1983) Anticipatory changes of long-latency stretch responses during preparation for directional hand movements. Brain Res 280:51–62.

Česonis J, Franklin DW (2020) Time-to-target simplifies optimal control of visuomotor feedback responses. eNeuro 7:ENEURO.0514-19.2020.

Chapman CE, Spidalieri G, Lamarre Y (1984) Discharge properties of area 5 neurones during arm movements triggered by sensory stimuli in the monkey. Brain Res 309:63–77.

Cheney PD, Fetz EE (1984) Corticomotoneuronal cells contribute to long-latency stretch reflexes in the rhesus monkey. J Physiol 349:249–272.

Churchland MM, Shenoy KV (2007) Delay of movement caused by disruption of cortical preparatory activity. J Neurophysiol 97:348–359.

Cisek P, Kalaska JF (2005) Neural correlates of reaching decisions in dorsal premotor cortex: specification of multiple direction choices and final selection of action. Neuron 45:801–814.

Cluff T, Scott SH (2013) Rapid feedback responses correlate with reach adaptation and properties of novel upper limb loads. J Neurosci 33:15903–15914.

Cluff T, Scott SH (2015) Apparent and actual trajectory control depend on the behavioral context in upper limb motor tasks. J Neurosci 35:12465–12476.

Cluff T, Crevecoeur F, Scott SH (2019) Tradeoffs in optimal control capture patterns of human sensorimotor control and adaptation. bioRxiv 730713. https://doi.org/10.1101/730713.

Conrad B, Matsunami K, Meyer-Lohmann J, Wiesendanger M, Brooks VB (1974) Cortical load compensation during voluntary elbow movements. Brain Res 71:507–514.

Conrad B, Meyer-Lohmann J, Matsunami K, Brooks VB (1975) Precentral unit activity following torque pulse injections into elbow movements. Brain Res 94:219–236.

Corneil BD, Munoz DP (2014) Overt responses during covert orienting. Neuron 82:1230–1243.

Corneil BD, Olivier E, Munoz DP (2004) Visual responses on neck muscles reveal selective gating that prevents express saccades. Neuron 42:831–841.

Crago PE, Houk JC, Hasan Z (1976) Regulatory actions of human stretch reflex. J Neurophysiol 39:925–935.

Crevecoeur F, Scott SH, Cluff T (2019) Robust control in human reaching movements: a model-free strategy to compensate for unpredictable disturbances. J Neurosci 39:8135–8148.

Cross KP, Cluff T, Takei T, Scott SH (2019) Visual feedback processing of the limb involves two distinct phases. J Neurosci 39:6751–6765.

Cross KP, Heming EA, Cook DJ, Scott SH (2020) Maintained representations of the ipsilateral and contralateral limbs during bimanual control in primary motor cortex. J Neurosci 40:6732–6747.

Cross KP, Cook DJ, Scott SH (2021) Convergence of proprioceptive and visual feedback on neurons in primary motor cortex. bioRxiv 442274. https://doi.org/10.1101/2021.05.01.442274.

Day BL (2014) Subcortical visuomotor control of human limb movement. In: Progress in Motor Control (Levin MF, ed), pp 55–68. New York: Springer.

Day BL, Brown P (2001) Evidence for subcortical involvement in the visual control of human reaching. Brain 124:1832–1840.

Dea M, Hamadjida A, Elgbeili G, Quessy S, Dancause N (2016) Different patterns of cortical inputs to subregions of the primary motor cortex hand representation in cebus apella. Cereb Cortex 26:1747–1761.

de Brouwer AJ, Jarvis T, Gallivan JP, Flanagan JR (2017) Parallel specification of visuomotor feedback gains during bimanual reaching to independent goals. eNeuro 4:ENEURO.0026-17.2017.

De Comite A, Crevecoeur F, Lefèvre P (2021) Online modification of goal-directed control in human reaching movements. J Neurophysiol 125:1883–1898.

Desmurget M, Epstein CM, Turner RS, Prablanc C, Alexander GE, Grafton ST (1999) Role of the posterior parietal cortex in updating reaching movements to a visual target. Nat Neurosci 2:563–567.

Diedrichsen J (2007) Optimal task-dependent changes of bimanual feedback control and adaptation. Curr Biol 17:1675–1679.

Dimitriou M, Franklin DW, Wolpert DM (2012) Task-dependent coordination of rapid bimanual motor responses. J Neurophysiol 107:890–901.

Dimitriou M, Wolpert DM, Franklin DW (2013) The temporal evolution of feedback gains rapidly update to task demands. J Neurosci 33:10898–10909.

Evarts EV, Tanji J (1976) Reflex and intended responses in motor cortex pyramidal tract neurons of monkey. J Neurophysiol 39:1069–1080.

Flash T, Hogan N (1985) The coordination of arm movements: an experimentally confirmed mathematical model. J Neurosci 5:1688–1703.

Franklin DW, Wolpert DM (2008) Specificity of reflex adaptation for task-relevant variability. J Neurosci 28:14165–14175.

Franklin S, Wolpert DM, Franklin DW (2017) Rapid visuomotor feedback gains are tuned to the task dynamics. J Neurophysiol 118:2711–2726.

Fromm C, Wise SP, Evarts EV (1984) Sensory response properties of pyramidal tract neurons in the precentral motor cortex and postcentral gyrus of the rhesus monkey. Exp Brain Res 54:177–185.

Gaveau V, Pisella L, Priot A-E, Fukui T, Rossetti Y, Pélisson D, Prablanc C (2014) Automatic online control of motor adjustments in reaching and grasping. Neuropsychologia 55:25–40.

Georgopoulos AP, Kalaska JF, Massey JT (1981) Spatial trajectories and reaction times of aimed movements: effects of practice, uncertainty, and change in target location. J Neurophysiol 46:725–743.

Goodale MA, Milner AD (1992) Separate visual pathways for perception and action. Trends Neurosci 15:20–25.

Gu C, Wood DK, Gribble PL, Corneil BD (2016) A trial-by-trial window into sensorimotor transformations in the human motor periphery. J Neurosci 36:8273–8282.

Hammond P (1956) The influence of prior instruction to the subject on an apparently involuntary neuro-muscular response. J Physiol 132:17–8P.

Heming EA, Cross KP, Takei T, Cook DJ, Scott SH (2019) Independent representations of ipsilateral and contralateral limbs in primary motor cortex. Elife 8:e48190.

Herter TM, Korbel T, Scott SH (2009) Comparison of neural responses in primary motor cortex to transient and continuous loads during posture. J Neurophysiol 101:150–163.

Jones EG, Coulter JD, Hendry SHC (1978) Intracortical connectivity of architectonic fields in the somatic sensory, motor and parietal cortex of monkeys. J Comp Neurol 181:291–347.

Kasuga S, Crevecoeur F, Cross KP, Balalaie P, Scott SH (2022) Integration of proprioceptive and visual feedback during online control of reaching. J Neurophysiol 127:354–372.

Keyser J, Medendorp WP, Selen LPJ (2017) Task-dependent vestibular feedback responses in reaching. J Neurophysiol 118:84–92.

Keyser J, Ramakers REFS, Medendorp WP, Selen LPJ (2019) Task-dependent responses to muscle vibration during reaching. Eur J Neurosci 49:1477–1490.

Knill DC, Bondada A, Chhabra M (2011) Flexible, task-dependent use of sensory feedback to control hand movements. J Neurosci 31:1219–1237.

Kozak RA, Kreyenmeier P, Gu C, Johnston K, Corneil BD (2019) Stimulus-locked responses on human upper limb muscles and corrective reaches are preferentially evoked by low spatial frequencies. eNeuro 6:ENEURO.0301-19.2019.

Kurtzer IL, Pruszynski JA, Scott SH (2008) Long-latency reflexes of the human arm reflect an internal model of limb dynamics. Curr Biol 18:449–453.

Lamarre Y, Spidalieri G, Chapman CE (1983) A comparison of neuronal discharge recorded in the sensori-motor cortex, parietal cortex and dentate nucleus of the monkey during arm movements triggered by light, sound or somesthetic stimuli. Exp Brain Res 49:140–156.

Latash ML (2012) The bliss of motor abundance. Exp Brain Res 217:1–5.

Lee RG, Tatton WG (1975) Motor responses to sudden limb displacements in primates with specific CNS lesions and in human patients with motor system disorders. Can J Neurol Sci 2:285–293.

Lemon RN, Mantel GW, Muir RB (1986) Corticospinal facilitation of hand muscles during voluntary movement in the conscious monkey. J Physiol 381:497–527.

London BM, Miller LE (2013) Responses of somatosensory area 2 neurons to actively and passively generated limb movements. J Neurophysiol 109:1505–1513.

Lowrey CR, Nashed JY, Scott SH (2017) Rapid and flexible whole body postural responses are evoked from perturbations to the upper limb during goal-directed reaching. J Neurophysiol 117:1070–1083.

Maeda RS, Cluff T, Gribble PL, Pruszynski JA (2018) Feedforward and feedback control share an internal model of the arm's dynamics. J Neurosci 38:10505–10514.

Maeda RS, Kersten R, Pruszynski JA (2020) Shared internal models for feedforward and feedback control of arm dynamics in non-human primates. Eur J Neurosci 53:1605–1620.

Marsden CD, Merton PA, Morton HB (1976) Servo action in the human thumb. J Physiol 257:1–44.

Matthews PB (1986) Observations on the automatic compensation of reflex gain on varying the pre-existing level of motor discharge in man. J Physiol 374:73–90.

Mutha PK, Sainburg RL (2009) Shared bimanual tasks elicit bimanual reflexes during movement. J Neurophysiol 102:3142–3155.

Nashed JY, Crevecoeur F, Scott SH (2012) Influence of the behavioral goal and environmental obstacles on rapid feedback responses. J Neurophysiol 108:999–1009.

Nashed JY, Crevecoeur F, Scott SH (2014) Rapid online selection between multiple motor plans. J Neurosci 34:1769–1780.

Omrani M, Pruszynski JA, Murnaghan CD, Scott SH (2014) Perturbation-evoked responses in primary motor cortex are modulated by behavioral context. J Neurophysiol 112:2985–3000.

Omrani M, Murnaghan CD, Pruszynski JA, Scott SH (2016) Distributed task-specific processing of somatosensory feedback for voluntary motor control. Elife 5:e13141.

Oostwoud Wijdenes L, Brenner E, Smeets JBJ (2011) Fast and fine-tuned corrections when the target of a hand movement is displaced. Exp Brain Res 214:453–462.

Philipp R, Hoffmann K-P (2014) Arm movements induced by electrical microstimulation in the superior colliculus of the macaque monkey. J Neurosci 34:3350–3363.

Picard N, Smith AM (1992) Primary motor cortical responses to perturbations of prehension in the monkey. J Neurophysiol 68:1882–1894.

Pisella L, Gréa H, Tilikete C, Vighetto A, Desmurget M, Rode G, Boisson D, Rossetti Y (2000) An 'automatic pilot' for the hand in human posterior parietal cortex: toward reinterpreting optic ataxia. Nat Neurosci 3:729–736.

Porter R, Lemon R (1993) Corticospinal function and voluntary movement. Oxford, UK: Clarendon Press.

Pruszynski JA, Kurtzer I, Scott SH (2008) Rapid motor responses are appropriately tuned to the metrics of a visuospatial task. J Neurophysiol 100:224–238.

Pruszynski JA, Kurtzer I, Lillicrap TP, Scott SH (2009) Temporal evolution of "automatic gain-scaling". J Neurophysiol 102:992–1003.

Pruszynski JA, King GL, Boisse L, Scott SH, Flanagan JR, Munoz DP (2010) Stimulus-locked responses on human arm muscles reveal a rapid neural pathway linking visual input to arm motor output: visual responses on human arm muscles. Eur J Neurosci 32:1049–1057.

Pruszynski JA, Kurtzer I, Nashed JY, Omrani M, Brouwer B, Scott SH (2011) Primary motor cortex underlies multi-joint integration for fast feedback control. Nature 478:387–390.

Pruszynski JA, Omrani M, Scott SH (2014) Goal-dependent modulation of fast feedback responses in primary motor cortex. J Neurosci 34:4608–4617.

Pruszynski JA, Johansson RS, Flanagan JR (2016) A rapid tactile-motor reflex automatically guides reaching toward handheld objects. Curr Biol 26:788–792.

Scholz JP, Schöner G (1999) The uncontrolled manifold concept: identifying control variables for a functional task. Exp Brain Res 126:289–306.

Scholz JP, Schöner G, Latash ML (2000) Identifying the control structure of multijoint coordination during pistol shooting. Exp Brain Res 135:382–404.

Scott SH (1999) Apparatus for measuring and perturbing shoulder and elbow joint positions and torques during reaching. J Neurosci Methods 89:119–127.

Scott SH (2004) Optimal feedback control and the neural basis of volitional motor control. Nat Rev Neurosci 5:532–546.

Sporns O, Edelman GM (1993) Solving Bernstein's problem: a proposal for the development of coordinated movement by selection. Child Dev 64:960–981.

Stavisky SD, Kao JC, Ryu SI, Shenoy KV (2017) Motor cortical visuomotor feedback activity is initially isolated from downstream targets in output-null neural state space dimensions. Neuron 95:195–208.e9.

Stein RB, Hunter IW, Lafontaine SR, Jones LA (1995) Analysis of short-latency reflexes in human elbow flexor muscles. J Neurophysiol 73:1900–1911.
Strick PL (1983) The influence of motor preparation on the response of cerebellar neurons to limb displacements. J Neurosci 3:2007–2020.
Stuphorn V, Hoffmann K-P, Miller LE (1999) Correlation of primate superior colliculus and reticular formation discharge with proximal limb muscle activity. J Neurophysiol 81:1978–1982.
Takei T, Crevecoeur F, Herter TM, Cross KP, Scott SH (2018) Correlations between primary motor cortex activity with recent past and future limb motion during unperturbed reaching. J Neurosci 38:7787–7799.
Takei T, Lomber SG, Cook DJ, Scott SH (2021) Transient deactivation of dorsal premotor cortex or parietal area 5 impairs feedback control of the limb in macaques. Curr Biol 31:1476–1487.e5.
Todorov E, Jordan MI (2002) Optimal feedback control as a theory of motor coordination. Nat Neurosci 5:1226–1235.
Weiler J, Gribble PL, Pruszynski JA (2015) Goal-dependent modulation of the long-latency stretch response at the shoulder, elbow, and wrist. J Neurophysiol 114:3242–3254.
Weiler J, Saravanamuttu J, Gribble PL, Pruszynski JA (2016) Coordinating long-latency stretch responses across the shoulder, elbow, and wrist during goal-directed reaching. J Neurophysiol 116:2236–2249.
Werner W (1993) Neurons in the primate superior colliculus are active before and during arm movements to visual targets. Eur J Neurosci 5:335–340.
Werner W, Hoffmann K-P, Dannenberg S (1997) Anatomical distribution of arm-movement-related neurons in the primate superior colliculus and underlying reticular formation in comparison with visual and saccadic cells. Exp Brain Res 115:206–216.
Wolpaw JR (1980) Amplitude of responses to perturbation in primate sensorimotor cortex as a function of task. J Neurophysiol 44:1139–1147.